Cell

Allogeneic CD19-targeted CAR-T therapy in patients with severe myositis and systemic sclerosis

Graphical abstract

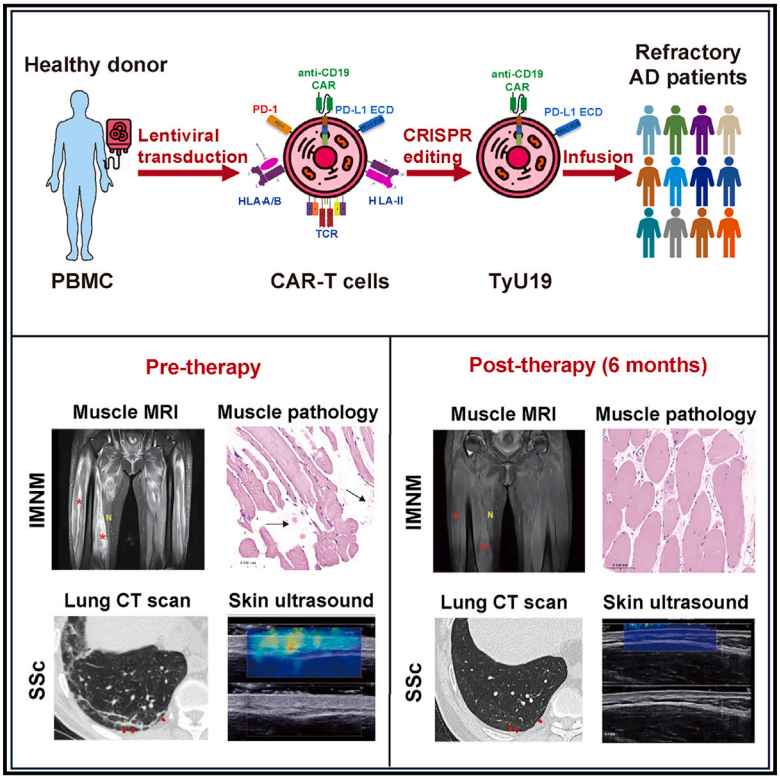

Highlights

- TyU19 is a genetically engineered, healthy donor-derived CD19-targeting CAR-T product
- TyU19 caused B cell depletion in three patients with refractory autoimmune diseases
- TyU19 alleviated severe skeletal muscle damage in a patient with refractory IMNM
- TyU19 reversed extensive fibrotic damage to critical organs in two patients with dcSSc

Authors

Xiaobing Wang, Xin Wu, Binghe Tan, ..., Huaxiang Wu, Bing Du, Huji Xu

Correspondence

myliu@bio.ecnu.edu.cn (M.L.), wuhx8855@zju.edu.cn (H.W.), bdu@bio.ecnu.edu.cn (B.D.), xuhuji@smmu.edu.cn (H.X.)

In brief

A genetically engineered, healthy donor-derived CD19-targeted chimeric antigen receptor (CAR)-T cell treatment achieved safe, deep remission in one patient with severe immune-mediated necrotizing myopathy and two patients with diffuse cutaneous systemic sclerosis, highlighting the potential of off-the-shelf CAR-T therapy in advancing clinical management of severe refractory autoimmune diseases.

Wang et al., 2024, Cell *187*, 4890–4904
September 5, 2024
https://doi.org/10.1016/j.cell.2024.06.027

CellPress

Cell

Article

Allogeneic CD19-targeted CAR-T therapy in patients with severe myositis and systemic sclerosis

Xiaobing Wang,[1,2,22] Xin Wu,[1,2,22] Binghe Tan,[3,4,22] Liang Zhu,[5,22] Yi Zhang,[1] Li Lin,[1,2] Yi Xiao,[6] An Sun,[6] Xinyi Wan,[6] Shiyuan Liu,[6] Yanfang Liu,[2,7] Na Ta,[7] Hang Zhang,[8] Jialin Song,[8] Ting Li,[1] Ling Zhou,[1] Jian Yin,[1] Lingying Ye,[1] Hongjuan Lu,[1] Jinwei Hong,[9] Hui Cheng,[9] Ping Wang,[9] Weiqing Li,[10] Jianfeng Chen,[3] Jin Zhang,[11] Jing Luo,[12] Miaozhen Huang,[12] Lehang Guo,[13] Xiaoming Pan,[14] Yi Jin,[15] Wenjing Ye,[16] Lie Dai,[17] Jian Zhu,[18] Lingyun Sun,[19] Biao Zheng,[4] Dali Li,[3,4] Yanran He,[20] Mingyao Liu,[3,4,*] Huaxiang Wu,[5,*] Bing Du,[3,4,*] and Huji Xu[1,2,12,21,23,*]

[1]Department of Rheumatology and Immunology, Shanghai Changzheng Hospital, Naval Medical University, Shanghai 200003, China
[2]National Key Laboratory for Immunity and Inflammation, Shanghai, China
[3]Shanghai Frontiers Science Center of Genome Editing and Cell Therapy, Shanghai Key Laboratory of Regulatory Biology and School of Life Sciences, East China Normal University, Shanghai 200241, China
[4]BRL Medicine Inc., Shanghai 201109, China
[5]Department of Rheumatology, the Second Affiliated Hospital, Zhejiang University School of Medicine, Hangzhou 310009, China
[6]Department of Radiology, Shanghai Changzheng Hospital, Naval Medical University, Shanghai 200003, China
[7]Department of Pathology, Shanghai Changhai Hospital, Naval Medical University, Shanghai 200082, China
[8]Department of Ultrasound, Shanghai Changzheng Hospital, Naval Medical University, Shanghai 200003, China
[9]Department of Rheumatology, The First Affiliated Hospital, Wenzhou Medical University, Wenzhou 325035, China
[10]Department of Pathology, Shanghai Changzheng Hospital, Naval Medical University, Shanghai 200003, China
[11]Department of Rheumatology and Clinical Immunology, Ningbo Medical Center Lihuili Hospital, Ningbo, Zhejiang 315040, China
[12]School of Medicine, Tsinghua University, Beijing 100084, China
[13]Department of Medical Ultrasound, Shanghai Tenth People's Hospital, School of Medicine, Tongji University, Shanghai 200072, China
[14]Department of Cardiology, Shanghai Changzheng Hospital, Naval Medical University, Shanghai 200003, China
[15]Department of Dermatology, Shanghai Changzheng Hospital, Naval Medical University, Shanghai Key Laboratory of Medical Mycology, Shanghai 200082, China
[16]Department of Rheumatology and Immunology, Shanghai Huashan Hospital, Fudan University, Shanghai 200040, China
[17]Department of Rheumatology, Sun Yat-Sen Memorial Hospital, Sun Yat-Sen University, Guangzhou 510120, China
[18]Department of Rheumatology and Immunology, The First Medical Center, Chinese PLA General Hospital, Beijing 100853, China
[19]Department of Rheumatology and Immunology, The Affiliated Drum Tower Hospital, Nanjing University Medical School, Nanjing 210008, China
[20]Committee on Cancer Biology, The University of Chicago, Chicago, IL 60637, USA
[21]Peking-Tsinghua Center for Life Sciences, Tsinghua University, Beijing 100084, China
[22]These authors contributed equally
[23]Lead contact
*Correspondence: myliu@bio.ecnu.edu.cn (M.L.), wuhx8855@zju.edu.cn (H.W.), bdu@bio.ecnu.edu.cn (B.D.), xuhuji@smmu.edu.cn (H.X.)
https://doi.org/10.1016/j.cell.2024.06.027

SUMMARY

Allogeneic chimeric antigen receptor (CAR)-T cells hold great promise for expanding the accessibility of CAR-T therapy, whereas the risks of allograft rejection have hampered its application. Here, we genetically engineered healthy-donor-derived, CD19-targeting CAR-T cells using CRISPR-Cas9 to address the issue of immune rejection and treated one patient with refractory immune-mediated necrotizing myopathy and two patients with diffuse cutaneous systemic sclerosis with these cells. This study was registered at ClinicalTrials.gov (NCT05859997). The infused cells persisted for over 3 months, achieving complete B cell depletion within 2 weeks of treatment. During the 6-month follow-up, we observed deep remission without cytokine release syndrome or other serious adverse events in all three patients, primarily shown by the significant improvement in the clinical response index scores for the two diseases, respectively, and supported by the observations of reversal of inflammation and fibrosis. Our results demonstrate the high safety and promising immune modulatory effect of the off-the-shelf CAR-T cells in treating severe refractory autoimmune diseases.

INTRODUCTION

Autoimmune diseases affect approximately 8% of the population,[1] and many have no cure and demand lifetime management. Despite advancements in various interventions, including biologics and targeted small molecules, many patients suffering from autoimmune diseases eventually relapse and sometimes develop complications that can become life threatening.[2] The majority of existing drugs, in addition to lacking curative potential, have substantial short-term and long-term toxicities; thus,

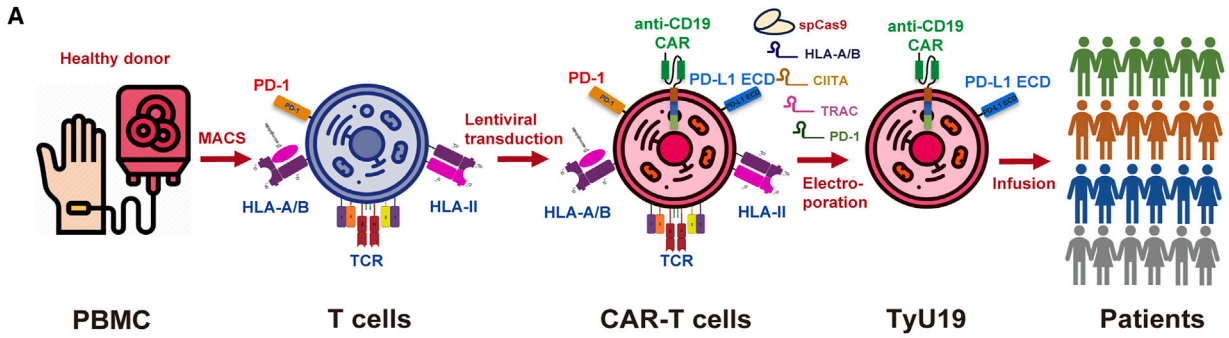

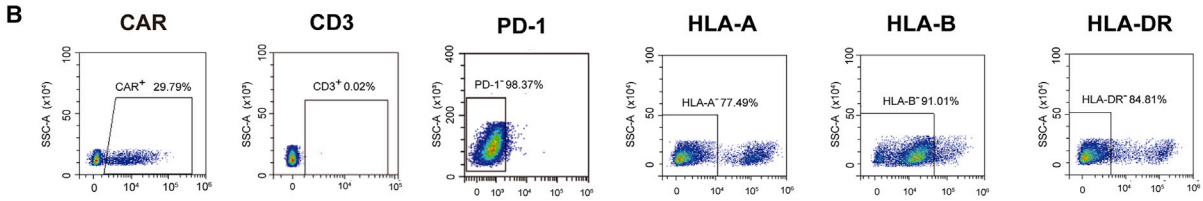

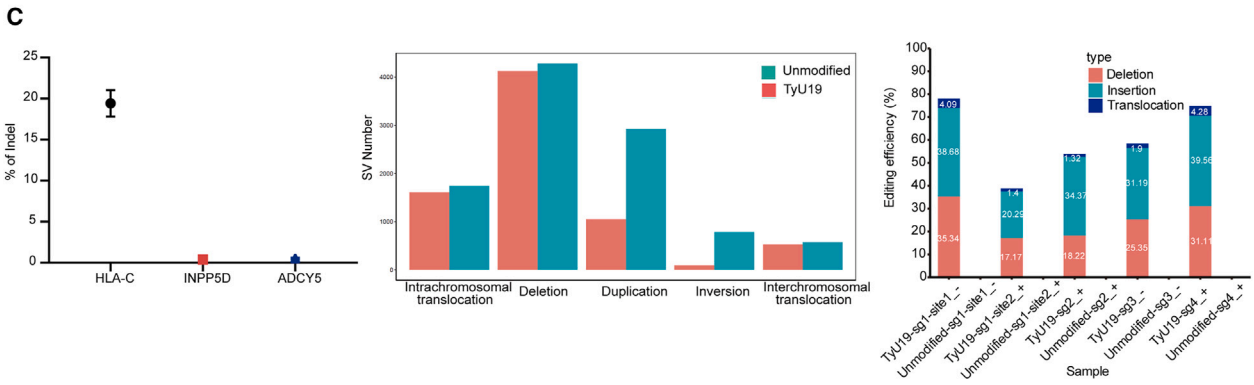

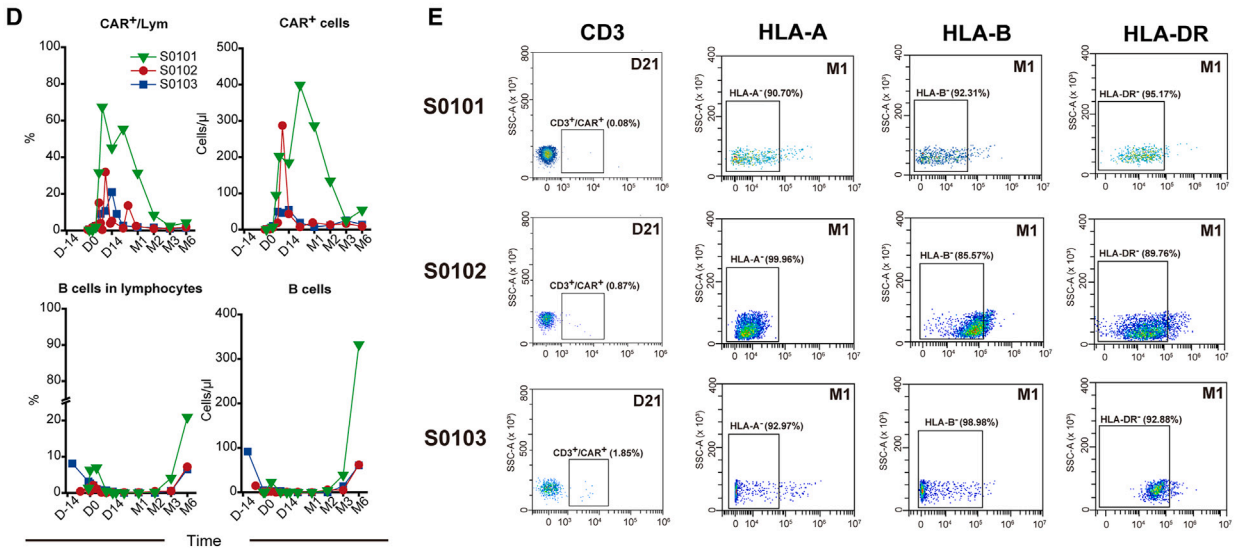

(legend continued on next page)

there are huge unmet medical needs for refractory autoimmune patients.

Immune-mediated necrotizing myopathy (IMNM) is a systemic autoimmune disease marked by myofiber necrosis and progressive weakness. One of the most aggressive subtypes of IMNM is signal recognition particle (SRP)-IMNM, which is characterized by anti-SRP autoantibody-driven immune attack of skeletal muscle. SRP-IMNM is particularly refractory to conventional therapies, and patients can rarely develop life-threatening systemic manifestations.[3–5] No treatment has been specifically approved for SRP-IMNM, and new treatment options are demanded.

Systemic sclerosis (SSc) is another autoimmune disease characterized by extensive fibrosis affecting various organs.[6] There are two main types of SSc: limited cutaneous SSc and diffuse cutaneous SSc (dcSSc),[7] with the latter associated with poor prognosis owing to aggressive disease development and early involvements of internal organ damage.[8] Conventional immunosuppressants may help to slow down the disease progression, yet the extensive fibrosis involving cardiovascular organs is generally considered irreversible.[9]

Autologous chimeric antigen receptor (CAR)-T therapy has been hailed as one of the greatest breakthroughs in the treatment of B cell malignancies, including refractory relapse leukemia and lymphomas.[10] Similar to B cell malignancies, autoantibody-related autoimmune diseases are rooted in developmental and functional abnormalities of the B cell compartment.[11]

Recent studies have explored the use of autologous CD19-targeted CAR-T therapies for treating autoimmune diseases and reported promising efficacy.[12–16] However, autologous CAR-T therapies are prohibitively expensive and vulnerable to failure during the manufacturing of personalized product. A scalable healthy donor-derived off-the-shelf product would greatly improve the accessibility of CAR-T.[17] Thus, the potential of applying allogeneic CAR-T products for treating refractory autoimmune diseases merits to be explored.

In this study, we have developed a healthy donor-derived, multiplex genome-edited allogeneic CD19-targeted CAR-T product for the treatment of 1 patient with refractory SRP-IMNM, and 2 patients with dcSSc. The treatment achieved deep B cell depletion and major clinical improvement by disease scoring in all patients that persisted throughout the 6-month monitoring period, with highly desirable safety profile. This study shows the potential of an off-the-shelf, allogeneic CAR-T product for the treatment of refractory autoimmune diseases.

RESULTS

Design and characterization of an allogeneic CD19-targeted CAR-T cell product, TyU19

The genetically engineered allogeneic CD19-targeted CAR-T cells (code name: TyU19) were produced according to the workflow illustrated in Figure 1A. Each batch started with 1×10^9 peripheral blood mononuclear cells (PBMCs), which was approximately 1/10 of a single donation from a healthy donor. T cells isolated from PBMCs were first transduced with lentivirus coding anti-CD19 CAR construct and then were knocked out for human leukocyte antigen (*HLA*)-*A*, *HLA-B*, class II major histocompatibility complex transactivator (*CIITA*), T cell receptor alpha constant (*TRAC*), and *PD-1* by electroporation-based CRISPR-Cas9 gene editing using Cas9 protein in complex with single guide RNAs (sgRNAs) for each target. Afterward, the T cells were expanded *in vitro* for 12 days. Finally, magnetic-activated cell sorting for purification of CD3-negative cells was performed to avoid graft-versus-host by the allogeneic T cells. Each batch typically yields >100 patient-use (1×10^6/kg CAR-positive cells per transfusion), and 1×10^8 CAR-positive TyU19 cells were cryopreserved in each aliquot to be used as an off-the-shelf product. The product from the batch used in this study is shown in Figure 1B. The percentage of CAR-positive cells was 29.79%, and the percentages of *TRAC*-knockout (by CD3-negative staining), *HLA-A and HLA-B* knockout (by HLA-A and B-negative staining), and *CIITA*-knockout (by HLA-DR-negative staining) were 99.80%, 77.49%, 91.01%, and 84.81%, respectively.

To check the potential off-target editing by the CRISPR-Cas9 system, GUIDE-seq, SITE-seq, and whole-genome sequencing (WGS) were used to identify off-target cleavage sites. As a result, 26 off-target cleavage sites were identified both by GUIDE-seq and SITE-seq, 3 of which were also identified by WGS (Table S1). The 3 overlapped *loci* sites identified by all 3 methods were then validated by site-specific amplification sequencing, which revealed ~20% indels in the *HLA-C* locus while close to background editing in the other 2 *loci*, including INPP5D and ADCY5 (Figure 1C, left). The off-target editing of HLA-C can be explained by its sequence homology with HLA-A/B, and the depletion of HLA-C shall not negatively impact the safety of the TyU19 product, only further reducing the immunogenicity of the product. Moreover, genetic stability was evaluated by WGS (Figure 1C, middle), and there was no higher level of chromosomal abnormalities in the TyU19 product than that in

Figure 1. Design and characterization of allogeneic CD19-targeted CAR-T cell product (TyU19) and corresponding changes in peripheral B cells

(A) Workflow of generating TyU19 cells.

(B) Flow cytometry for evaluation of surface marker expression in TyU19 product.

(C) Site-specific amplification sequencing of potential cleavage sites (left); chromosomal structural variation evaluated by whole-genome sequencing (WGS) in both TyU19 cells and unmodified T cells (middle); quantification of gene editing outcomes in TyU19 cells by primer extension-mediated sequencing (PEM-seq) (right). Bar plot shows the editing efficiency of samples. Deletion, insertion, and translocation events were identified by PEM-seq.

(D) Flow cytometry of surface marker expression in CAR+ cells *in vivo*. CD3 expression in CAR+ cells from peripheral blood harvested at day 21 (D21) after transfusion. HLA-A/-B/-DR expression in CAR+ cells from peripheral blood harvested at 1 month (M1) after transfusion. Top, patient S0101; middle, patient S0102; bottom, patient S0103.

(E) The percentages and absolute numbers of CAR+ cells and B cells. Flow cytometry of circulating CAR+ cells at the indicated time point post-infusion, displayed by the percentage of CAR+/CD45+ lymphocytes or by absolute cell numbers per μL (top). Peripheral B cells were displayed by the percentage of CD19+/CD45+ lymphocytes or by the absolute number per μL (bottom). Data from 3 cases, up to 6 months' follow-up.

See also Figure S1 and Table S1.

the unedited control cells. Finally, primer extension-mediated sequencing (PEM-seq) was further used to comprehensively quantify DNA repair outcomes of gene editing in TyU19 cells (Figure 1C, right). The majority of the events were on-target editing resulted in deletions and insertions close to double-strand break (DSB). For editing with different sgRNA, approximately 1%–4% translocation events were discovered, none of which have been linked with oncogenic mutations nor significantly compromise the overall genetic stability in the edited product.

The genetic modifications among CAR-positive cells after treatment were assessed by flow cytometry in all three patients. For patients S0101, S0102, and S0103, CD3 negativity rates at the peak of CAR-T cell expansion were 99.92%, 99.13%, and 98.15%, respectively, on day 21. This indicates a minimal risk for graft-versus-host disease (GVHD). HLA expression levels 1-month post treatment showed that the negative rates for HLA-A, HLA-B, and HLA-DR were 90.70%, 92.31%, and 95.17% for S0101; 99.96%, 85.57%, and 89.76% for S0102; and 92.97%, 98.98%, and 92.88% for S0103, as depicted in Figure 1D.

Patients with refractory autoimmune diseases were recruited to be treated with TyU19

A case of SRP-IMNM and two cases of dcSSc were recruited in this study for an investigator-initiated trial conducted at our institution using TyU19 for the treatment of refractory relapse autoimmune diseases (NCT05859997).

The first patient recruited was a 42-year-old female with severe refractory SRP-IMNM (S0101). She was first diagnosed with SRP-IMNM in 2013 after experiencing severe cervical and proximal muscle weakness and a high fever, and she tested positive for anti-SRP autoantibody and had a creatine kinase (CK) level higher than 10,000 U/L. The diagnosis was confirmed by thigh muscle biopsy, which showed patchy myonecrosis and regenerating myofiber. The patient had been taking prednisone daily (dose ranging from 10–80 mg) for the past 10 years and had received various immunosuppressants in combination successively. Intravenous immunoglobulin (IVIG) had been used frequently as an adjuvant therapy, and the patient had received advanced treatments including prednisone pulse therapy (500 mg per day for 3 days) during one previous episode (Table 1). Regardless of temporary and moderate alleviation of disease symptoms, none of the previous attempts brought autoantibody nor CK levels to normal level. In March 2023, the patient had another major flare and experienced debilitating symmetrical proximal weakness. Treatment with IVIG (20 g/day for 3 days) at the beginning of the episode, followed by 100 mg cyclosporin A twice per day and 12.5 mg methotrexate once per week in combination with 60 mg prednisone daily only reduced her CK level from 9,536 to 3,700 U/L, and her muscle strength continued to deteriorate according to MMT-8 scoring. Because of the patient's rapid disease progression despite of extensive therapeutic interventions, she was qualified for recruitment to be treated with allogeneic CAR-T in our trial. Informed consent in accordance with the declaration of Helsinki was obtained in writing by the patient. She started the preconditioning for treatment on May 22, 2023.

The second (S0102) and the third (S0103) patient recruited on June 27 and August 3, 2023 were both middle-aged male with severe dcSSc. Both patients were positive for anti-Scl-70 autoantibody and had systemic involvements including fibrotic damage to the skin, heart, lung, and gastrointestinal tract (Table 1). Upon enrollment, the heart and lung functions in patient S0102 were rapidly deteriorating regardless of aggressive treatments including prednisone pulse therapy and biologics targeting aberrantly activated B cells like Belimumab and Telitacicept (Table 1). Patient S0102 had digital ulcer and nailfold capillaroscopy showed a reduction in capillary count and twisted capillary structure, while in patient S0103, the capillary structures appeared to be dilated and hemorrhagic (Figure S1A). Histopathological analysis of the skin biopsy from the upper arms indicated collagen degeneration especially in patient S0102, while patient S0103 was characterized by augmented density and compact arrangement of dermal collagen fibers (Figure S1B). Patient S0103 was experiencing painful, debilitating, and rapidly progressing skin stiffness that restricted him from simple daily activities like raising hands and dressing himself. Both patients were recruited with written consent upon enrollment and before treatments.

Allogenic CD19-targeted CAR-T therapy and follow-up scheme

Upon enrollment, all immunosuppressants were stopped before the planned TyU19 infusion except for glucocorticoids, which were gradually tapered down from 50 to 15 mg/day over the course of 5 days. Before dosing the patients intravenously with 1×10^6 cells/kg CAR-positive TyU19 cells, the patients received a standard preconditioning regimen (in accordance with approved autologous CAR-T products) involving 25 mg/day/m^2 Fludarabine from day-5 (5 days before infusion) to day-3 and 300 mg/day/m^2 cyclophosphamide on day-5 and day-4 for lymphodepletion. Each patient underwent systematic follow-up assessments for efficacy and safety on the 14^{th} day (day 14), on 1-month (M1), 2-month (M2), 3-month (M3), and 6-month (M6) (for all 3 patients) intervals after TyU19 infusion.

Allogeneic CD19-targeted CAR-T cells expanded after transfusion and eradicated B cells

After infusion, the percentage of CAR-positive cells among CD45-positive lymphocytes in the patient's blood was monitored using flow cytometry and staining CAR by CD19-fluorescein isothiocyanate (FITC). For subject S0101, the percentage of CAR-positive cells significantly increased within the first week after infusion, peaked at 67.38% on day 8, and dropped to 45.09% on day 14. On day 21, there was another significant increase in the percentage of CAR-positive cells, indicating successful *in vivo* expansion of implanted cells. The percentage of CAR-positive cells gradually dropped to 31.49%, 8.43%, 2.46%, and 4.37% at M1, M2, M3, and M6 follow-up, respectively (Figure 1E, top left). Consistent with the trends observed for the percentage of CAR-positive cells, the number of CAR-positive cells peaked at 398.8 cells/μL on day 21 and decreased to 134, 25.34, and 53.75 cells/μL at M2, M3, and M6, respectively (Figure 1E, top right). For patients S0102 and S0103, after infusion, there was a marked increase in both the percentage and absolute number of CAR-positive cells. For S0102, the peak was observed on day 10 (31.9%); for patient S0103, the peak was reached on day 14 (21.01%) (Figure 1E, top). Regarding B cell depletion, for

Table 1. Characteristics of patients at baseline

	Case1 (S0101)	Case 2 (S0102)	Case 3 (S0103)
Demographics			
Age (years)	42	45	56
Sex (female/male)	female	male	male
Disease duration (years)	10	3	1
Disease progressing(yes/no)	yes	yes	yes
Laboratory values			
Baseline SRP (AU)	+ (12)	–	–
Baseline Scl-70 (AU)	–	+ (100)	+ (66)
Baseline IgG (g/L)	8.75	12.1	14.6
Baseline hemoglobin (g/dL)	140	87	136
Baseline white blood cells (N/μL)	15.2	6.4	4.2
Baseline lymphocytes (N/μL)	2.2	1.99	1.08
Baseline platelets (N/μL)	260	393	138
Baseline B cells (N/μL)	109	5	92
Organ involvements			
Muscle (presence/absence)	+	–	–
Skin (presence/absence)	–	+	+
Lungs (presence/absence)	–	+	+
Heart (presence/absence)	–	+	+
Digital ulcer (presence/absence)	–	+	–
Gastrointestinal tract (presence/absence)	–	+	+
Previous treatment history			
Glucocorticoid (yes/no)	prednisone 10–80 mg/day, for 10 years; 500 mg/day, for 3 days	prednisone 5–40 mg/day, for 3 years	methylprednisolone 24–40 mg/day, for 6 months
Cyclophosphamide (yes/no)	0.4 g every 2 weeks for 3 months, followed by 0.4 g monthly for the subsequent 3 months	0.5 g every 2 weeks for 3 months, followed by 0.5 g monthly for the subsequent 9 months	0.5 g every 2 weeks for 3 months, followed by 0.5 g monthly for the subsequent 3 months
Hydroxychloroquine (yes/no)	200 mg bid, for 6 years	200 mg bid, for 3 years	N/A
Mycophenolate (yes/no)	500–1,000 mg/day, for 6 years	500–1,000 mg/day, for 2 years	250 mg/day, for 3 months
Tacrolimus (yes/no)	3 mg/day, for 1 year	N/A	1 mg/day, for 1 month
Tocilizumab (yes/no)	480–560 mg, intravenous drip, every month, for 6 months	480–560 mg, intravenous drip, every month, for 6 months	162 mg, hypodermic injection, every 2 weeks, for 4 months
B cell depletion (yes/no)	N/A	Belimumab (400 mg intravenous drip every month, for 3 months), telitacicept (80 mg, hypodermic injection, every week, for 3 months)	N/A
Other (yes/no)	Abatacept (80 mg hypodermic injection every week, for 3 months, 2 years), Azathioprine (50 mg/day, for 3 years), Cyclosporin A (100 mg bid, for 1 month), intravenous immunoglobulin (20 g/day × 3 day intravenous drip, many times), Methotrexate (12.5 mg every week, for 1 month)	Rapamycin 1 mg/day, plasmapheresis (7 times in 1 year), mesenchymal stem cell transplantation	N/A

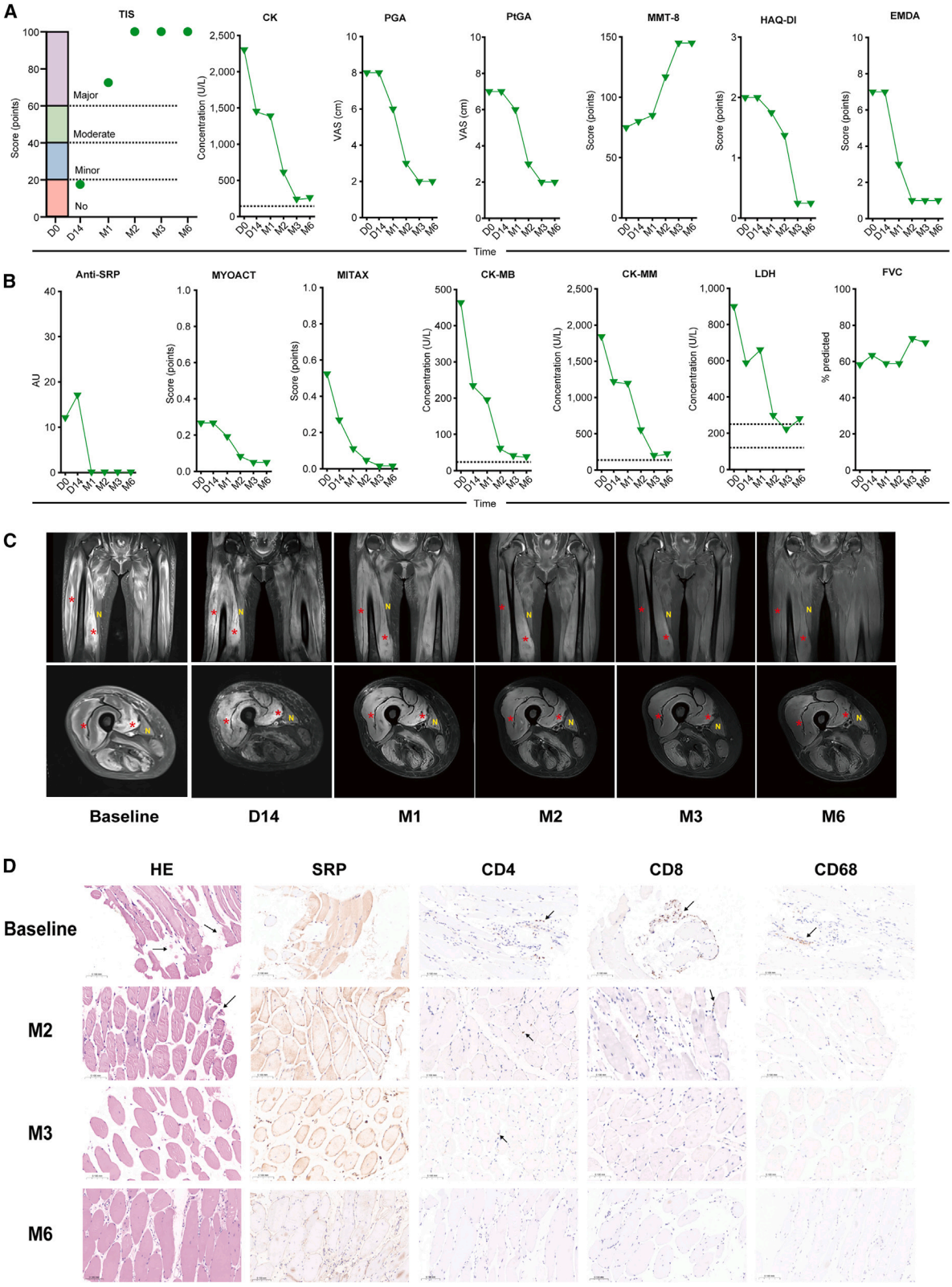

(legend on next page)

S0101, the preconditioning effectively depleted all circulating B cells at the time of infusion, yet the B cells quickly grew back shortly after the retraction of preconditioning drugs (Figure 1E, bottom). Nevertheless, in accordance with the expansion of CAR-positive cells, the absolute circulating B cell counts and percentage of B cells in lymphocytes quickly dropped to undetectable level by flow cytometry again, and the deep B cell aplasia was maintained for almost 2 months. With CAR-positive cells dropped to a very low level 2 months after the transfusion, B cells gradually recovered to the normal range by the M6 follow-up. For S0102, B cell counts fell from 5 cells/μL pre-therapy to 0 at M1 and recovered to 5 cells/μL by M3, and 62 cells/μL by M6. For S0103, B cell counts decreased from 92 to 1 cell/μL within 2 weeks after treatment and remained very low in number for about 2 months, and then recovered to 14 cells/μL at M3 and 61 cells/μL by M6, respectively (Figure 1E, bottom).

Clinical improvements following allogeneic CD19-targeted CAR-T cell treatment

Improvement in SRP-IMNM patients by total improvement score and other clinical score measurements

For S0101 with SRP-IMNM, the clinical improvement was evaluated by total improvement score (TIS).[18] As shown in Figure 2A, the patient exhibited major clinical improvement at M1 (TIS: 72.5), complete remission (TIS ∼100) at M2, and remained in complete remission at M6 after the treatment. The concentrations of CK decreased from 2,295 U/L at the time of treatment to 1,383 U/L at M1 and 606 U/L at M2, and finally fell close to the normal range at M3 (234 U/L) and M6 (255 U/L) (Figure 2A). There was significant improvement in physician global assessment (PGA) and patient global assessment (PtGA) scores since day 14 after treatment, reaching to VAS score 2 at M3 and maintaining it to M6 (Figure 2A). The patient regained muscle strength, with the MMT-8 test score increasing from 75/150 at baseline to 85/150, 117/150, 145/150, and 143/150 at M1, M2, M3, and M6, respectively (Figure 2A). These profound improvements were accompanied by enhanced quality of life, as indicated by the Health Assessment Questionnaire Disability Index (HAQ-DI), which decreased from 2 at the baseline to 1.75 at M1, 0.25 at M3, and M6 (Figure 2A). The extramuscular disease activity, as indicated by extramuscular activity (EMDA), decreased from 7 to 1 at M2, and the efficacy was maintained from M3 to M6 (Figure 2A).

There were also improvements in the other clinical measurements, most notably in anti-SRP antibody, which had a baseline level of 12 AU but was completely absent after 1 month and remained undetectable even after B cells were restored to normal range at M6 (Figure 2B). Myositis activity as measured by Myositis Disease Activity Assessment Visual Analogue Scales (MYOACT) and Myositis Intention to Treat Activity Index (MITAX)[19] was also significantly improved (Figure 2B), and the concentrations of markers for muscle damage (CK-MB, CK-MM, and lactate dehydrogenase) were greatly reduced after 1 month and continued to improve throughout the monitoring period (Figure 2B).

Improvement of myositis by imaging and pathological changes

The baseline muscle MRI images, taken in a coronal view using a fat-suppressed sequence of both thighs, revealed patchy and asymmetric edema within the thigh muscles, showing areas of hyperintensity. Axial views further highlighted muscle hyperintensity indicative of inflammatory infiltration, primarily affecting the adductor magnus and vastus lateralis muscles, in contrast to the surrounding normal sartorius muscles. Additionally, high signal intensities due to edema within the subcutaneous fascia were also noted (Figure 2C).

During the 6-month follow-up after therapy, imaging showed a significant trend toward resolution, marked by a gradual reduction in the intensity of thigh edema signals compared with the adjacent normal sartorius muscle. This reduction was particularly notable in the adductor magnus muscle and was accompanied by an improvement in thigh muscle atrophy. These findings suggest a positive response to the therapeutic intervention (Figure 2C).

Finally, the presence of patchy muscle necrosis accompanied by infiltration of immune cells and an elevated expression of SRP in the thigh muscle biopsy was confirmed at the baseline as assessed by H&E and immunohistochemistry staining. The pathological damage notably ameliorated in the follow-ups and appeared to be mostly resolved at M6 follow-up, accompanied by a substantial decrease in SRP expression and disappearance of infiltrated lymphocytes, including CD4+ and CD8+ T cells and CD68+ macrophages (Figure 2D).

Improvement in dcSSc by composite response index scoring

For dcSSc, the clinical improvement from the baseline was primarily evaluated using the American College of Rheumatology Composite Response Index in Systemic Sclerosis (ACR-CRISS) score, which includes the modified Rodnan skin score (mRSS),[20] forced vital capacity (FVC), HAQ-DI, PGA score, and PtGA score. An ACR-CRISS score $\geq$ 0.6 is considered an improvement, while a score $<$ 0.6 indicates no improvement.[21] The response

Figure 2. Efficacy of TyU19 intervention for refractory IMNM

(A) Primary clinical improvement assessment. The ACR/EULAR total improvement score (TIS) consists of creatinine kinase (CK) concentration, physician global assessment (PGA) score, patient global assessment (PtGA) score, manual muscle testing-8 (MMT-8) score, Health Assessment Questionnaire Disability Index (HAQ-DI) score, and extramuscular activity (EMDA).

(B) Additional clinical improvement assessments. Myositis Disease Activity Assessment Visual Analogue Scales (MYOACT), Myositis Intention to Treat Activity Index (MITAX), anti-SRP autoantibody levels, CK-MB, CK-MM, and lactate dehydrogenase (LDH) concentration, and forced vital capacity (FVC).

(C) Representative MRI scans of fat suppression sequences of the patient's thigh muscle (coronal and axial). At baseline, diffuse heterogeneous signal intensification suggested muscle edema, especially in the adductor magnus and vastus lateralis muscles (marked by red stars). The gracilis and sartorius muscles showed normal signals (marked by N). Post-TyU19 intervention, affected muscles display reduced edema and more uniform signals, aligning more closely with the normal sartorius muscle (N). Top: coronal view; bottom: axial view.

(D) H&E staining of the thigh muscle biopsy at baseline, M2, M3, and M6 post treatment. Immunohistochemistry evaluation showing the level of SRP, CD4+ and CD8+ T cells, and CD68+ macrophage infiltration in the muscle biopsy.

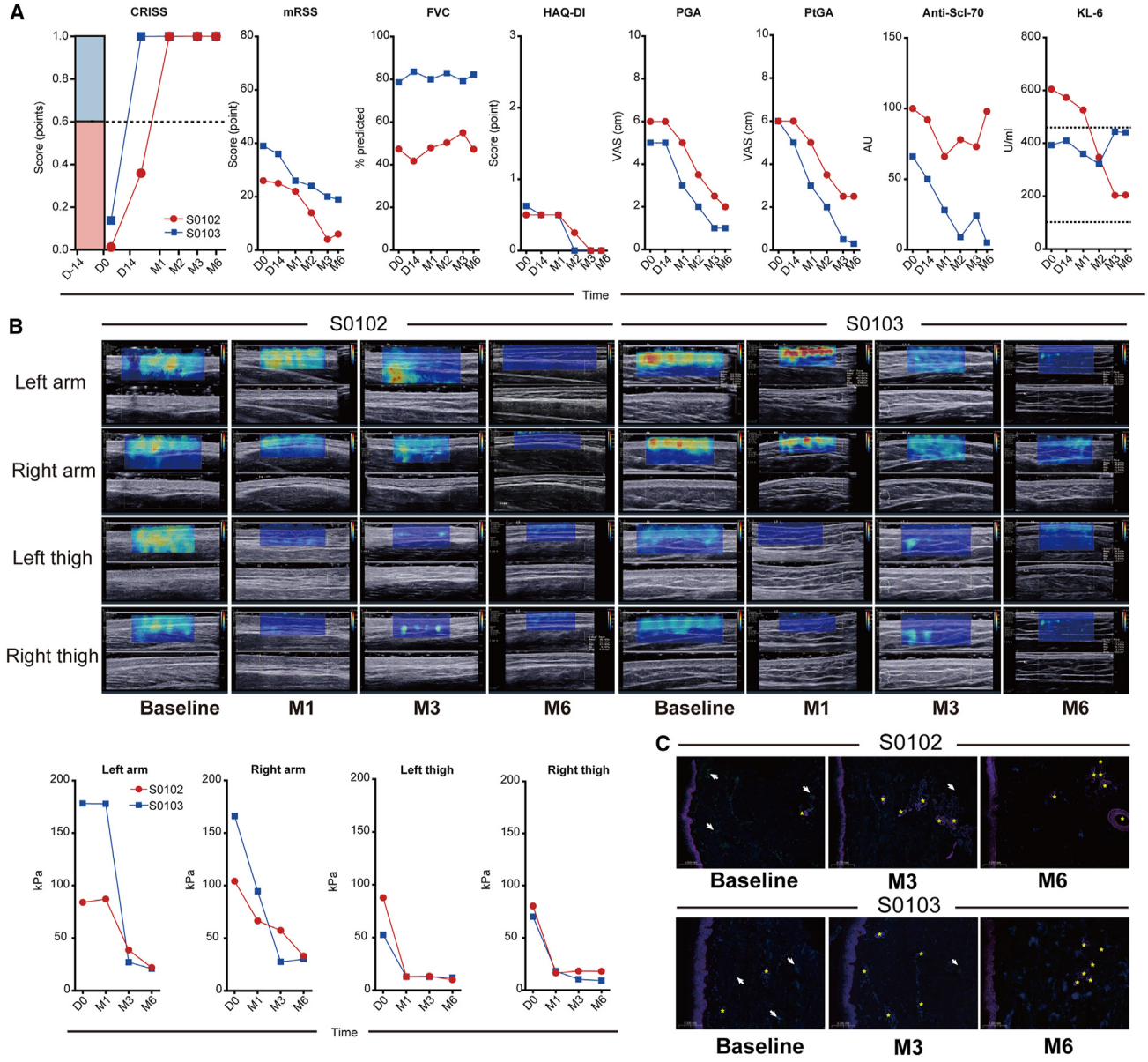

Figure 3. Efficacy of TyU19 intervention in refractory dcSSc patients and its effect on skin condition

(A) Major clinical improvement assessments using the American College of Rheumatology Combined Response Index in Systemic Sclerosis (ACR-CRISS), which includes the modified Rodnan skin score (mRSS), forced vital capacity (FVC), Health Assessment Questionnaire-Disability Index (HAQ-DI), physician global assessment (PGA), patient global assessment (PtGA), and serum levels of anti-Scl-70 autoantibody and KL-6.

(B) Assessment of skin elasticity and stiffness by ultrasound skin elastography. Left, elastographic color maps (red hue indicates harder tissue and blue hue indicates softer tissue). Right, elastographic measurements of skin stiffness values.

(C) Skin biopsy analysis using multi-color immunofluorescence histochemistry at the baseline, M3 and M6 follow-up. Skin follicles and sudoriferous glands were noted by yellow asterisks, and the expression of TGF-β was indicated by white arrows. Top, patient S0102; bottom, patient S0103.

See also Figure S1.

to TyU19 intervention was primarily assessed using the ACR-CRISS (Figure 3A). Patient S0102 reached an ACR-CRISS score of 0.998 at M2, 1.0 at M3, and 0.999 at M6. Patient S0103 achieved an ACR-CRISS score of 0.996 at M1, which increased to 0.999 at M2 and remained the same at M3 and M6. Using the revised CRISS assessment,[22] patient S0103 demonstrated improvement of at least 25%, 50%, and 75% in three or more of the five core items at both M3 and M6 follow-up visits. Conversely, patient S0102, initially presenting with severe illness, exhibited improvement of at least 25% and 50% in three or more of the five core items at both M3 and M6. Following treatment, there was a significant decrease in anti-Scl-70 autoantibody levels in both patients, with near-complete elimination achieved in patient S0103 by M6. The components of

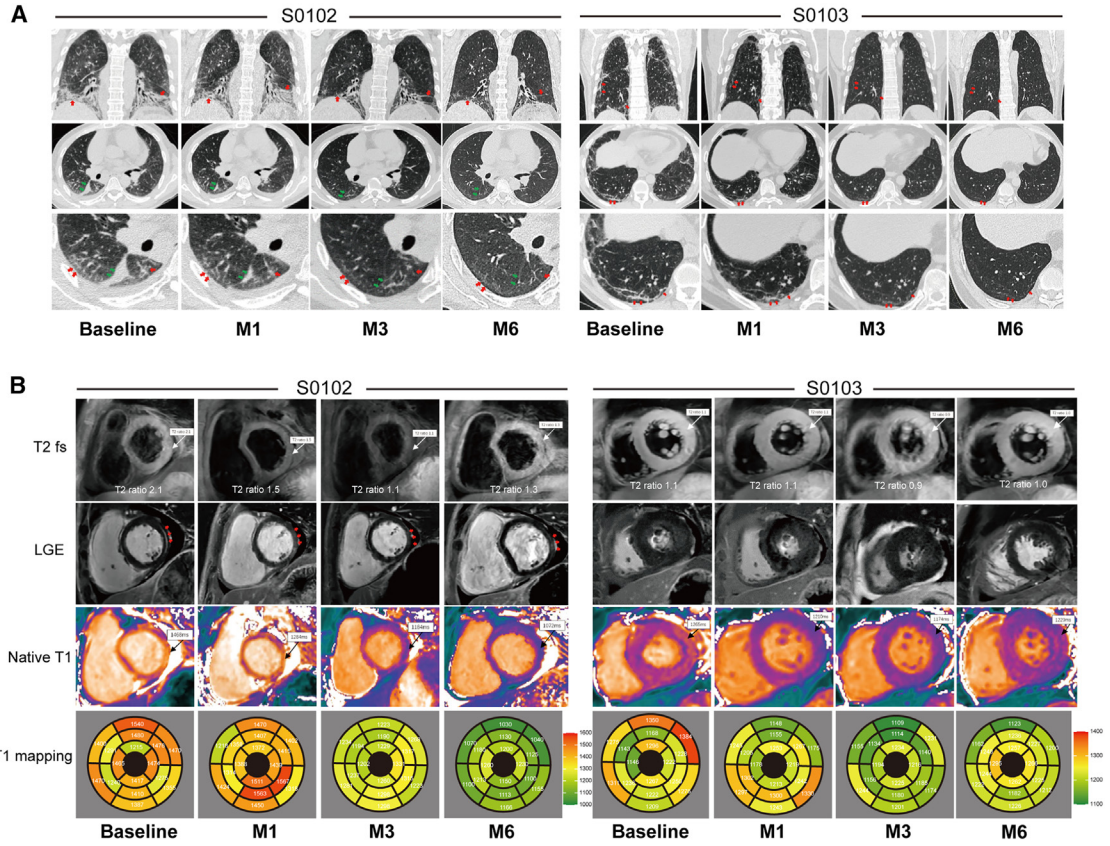

Figure 4. Effects of TyU19 intervention on lung and heart involvement in refractory dcSSc patients

(A) High-resolution CT (HRCT) scans demonstrated improvement in pulmonary inflammation and fibrosis following TyU19 intervention in both patients. Left, patient S0102, patchy and linear opacities (indicated by thick red arrows), interlobar effusion (marked by green arrows); right, patient S0103, fibrous linear shadows (indicated by red arrows).

(B) Cardiac magnetic resonance (CMR) to show amelioration of myocardial inflammation and fibrosis following TyU19 intervention, especially in patient S0102. Left, patient S0102; right, patient S0103. Bottom: A bull's-eye plot illustrating a decrease in T1 mapping values across all myocardial segments in both patients after TyU19 intervention.

ACR-CRISS, mRSS, PGA, and PtGA were significantly lower at M6 when compared with the scores at the baseline in both patients. Although patient S0102 experienced only a temporary decrease in anti-Scl-70 autoantibody levels, improvement was noted in most other clinical measurements (Figure 3A).

Improvement in dcSSc by reversal of skin fibrosis

The mRSS scores for S0102 decreased from 26 at baseline to 22 at M1, 4 by M3, and 6 by M6. For S0103, whose skin hardening was prominent and rapidly progressing, the scores decreased from an initial high of 39 to 26 at M1, and further decreased to 20 at M3 and 19 at M6 (Figure 3A). Skin elasticity was further measured by wave elastography,[23] and the elastographic color map from skin elastography revealed a transition from predominantly hard (red) tissue to softer (blue) tissue, indicating reduced stiffness. At M1 the elasticity of skin on the thighs was normal in both patients (Figure 3B). Additionally, skin biopsies were obtained from the lateral side of the right forearm at baseline and again 6 months post treatment. Pathological morphology of the skin showed gradual improvement after treatment, as evidenced by multi-color immunofluorescence histochemistry. Specifically, patient S0102, initially presenting with follicular atrophy and a limited number of sudoriferous glands, exhibited significant hair follicle regeneration and gland rejuvenation during the 6-month follow-up (Figure 3C). Furthermore, a decrease in transforming growth factor-beta (TGF-β) levels in the dermis of the forearm skin was also observed after intervention with TyU19. The immunohistochemistry further demonstrated that B cells were eliminated from the skin in both cases at the 3-month follow-up and remained negative in the skin at the 6-month follow-up even after the recovery of normal peripheral B cell levels (Figure S1C).

Improvement in dcSSc by the reversal of lung fibrosis and inflammation

The severity of interstitial lung disease (ILD) was assessed by chest computed tomography (CT) scans, lung function test, and serum concentration of KL-6. For patient S0102, axial and coronal chest high-resolution CT (HRCT) scans revealed multiple patchy and linear opacities in both lungs, accompanied by thickened interlobular septa (Figure 4A). The bilateral pulmonary inflammation, interlobar effusion, and fibrous strands were markedly reduced by the M1 follow-up and significantly improved by the M3 follow-up, which was largely maintained by the M6 follow-up.

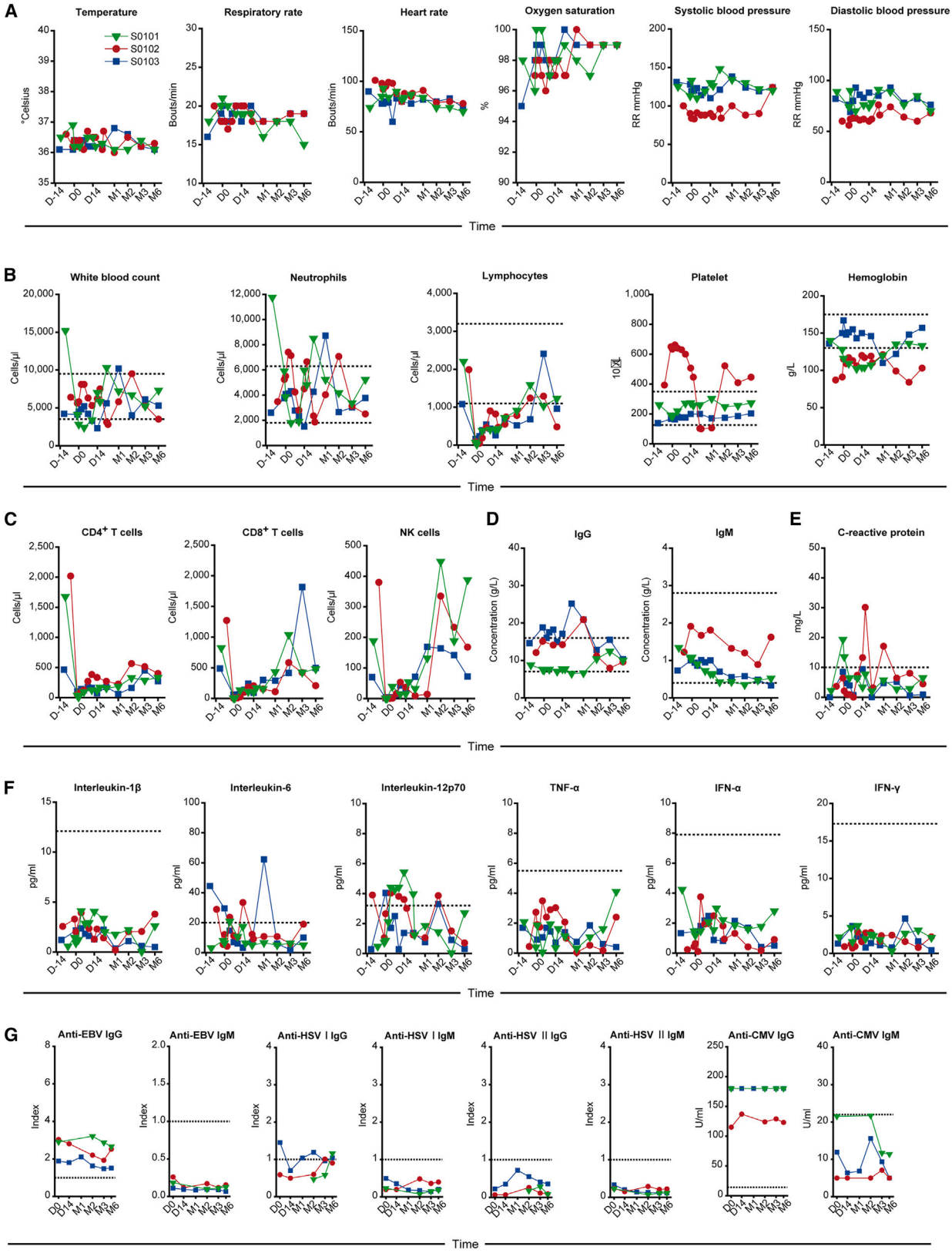

(legend on next page)

Although the functional improvement in the lung was mild by FVC measurement (Figure 3A), patient S0102 experienced drastic decrease in KL-6 from 605 U/mL at baseline to the normal level of 203 U/mL at M3, which was maintained at 204 U/mL at M6, indicating significant improvement in fibrotic lung lesions (Figure 3A). Patient S0103 had much lower lung involvement than patient S0102. HRCT scan showed fibrous linear opacities in the posterior basal segment of the right lower lobe and ground-glass opacities within the alveoli of the right upper lobe, which was largely resolved by the M3 follow-up and was largely maintained at the M6 follow-up. Functional measurement by FVC and levels of fibrotic lesion marker KL-6 in S0103 were mostly within the normal range (Figure 3A).

Improvement in dcSSc by the reversal of cardiac involvement

Cardiac lesions were measured by cardiac magnetic resonance (CMR). In S0102, at the baseline, there was extensive edema and fibrosis in the heart, especially in the left ventricular wall revealed by T2-weighted inversion-recovery imaging and late gadolinium enhancement (LGE) (Figure 4B, top 2). Significant edema absorption was observed at M1 (T2 ratio decreased from 2.1 to 1.5), and the LGE was almost fully resolved, accompanied by a decrease in naive T1 values in the affected area. Myocardial T1 mapping across various segments was conducted, and the resulting values were represented as bull's-eye plots (Figure 4B, bottom). A general decrease in these values was observed. All these effects persisting until M6. In patient S0103, baseline CMR images revealed less severe heart involvement compared with S0102, without obvious LGE (Figure 4B, top 2). An elevated native T1 and T2 values in the left ventricular lateral wall (focal T1 = 1,265 ms, focal T2 = 55 ms; compared with normal cutoff values: T1 $\leq$ 1,140 ms, T2 $\leq$ 54 ms), suggesting acute myocardial injury. At M6 follow-up, there was a significant reduction in the native T1 values of the left ventricular lateral wall (1,229 ms). After TyU19 intervention, he also showed reduced T1 mapping values across all myocardial segments, suggesting diminished cardiac fibrosis (Figure 4B, bottom).

Safety profiling following allogeneic CD19-targeted CAR-T cell treatment

In our study, none of our three patients displayed manifestations indicative of CRS, as per the ASTCT CRS Consensus Grading criteria. Any signs of acute GVHD according to the 2016 Mount Sinai criteria and signs of chronic GVHD according to the 2020 NCCN guidelines were closely monitored, yet no relevant clinical symptoms happened histological manifestations such as interface dermatitis, apoptosis of keratinocytes, lymphocytic infiltrate, and dermal sclerosis in skin tissue were observed, and therefore all patients scored 0 in GVHD-related side effects. All of the patients' vital signs remained mostly stable throughout the monitoring period (Figure 5A), besides temporal lymphopenia due to pre-conditioning (Figure 5B). T cells and NK cells were firstly depleted by preconditioning, and by the M2 follow-up, CD8+ T cells and NK cells mostly resumed the level before preconditioning in all 3 cases (Figure 5C). The immunoglobulin (Ig) levels, including IgG and IgM, were both maintained above the lower limit of the normal range throughout the treatment period, probably due to the long half-lives of IgGs, keeping the patients safe during the temporal B cell aplasia induced by the treatment (Figure 5D). Notably, the level of protective antibodies against viral infections was also not significantly impacted by the CAR-T treatment (Figure 5G).

There was a small fluctuation in the C-reactive protein (CRP) level during the lymphodepletion period in S0101 and another small fluctuation immediately following the TyU19 infusion in S0101 and S0102, without any noticeable clinical symptoms (Figure 5E). No significant upregulation of any CRS-related cytokines was observed throughout the monitoring period in S0101 (Figure 5F). Most cytokine levels were within the normal range, except for IL-6, which was elevated in S0103 at M1, and IL-12, which was elevated in S0102 within the first 2 weeks after treatment. Nevertheless, all patients experienced no relevant clinical symptoms.

DISCUSSION

In this study, we present the very first use of off-the-shelf allogeneic CD19-targeted CAR-T cells in human for the treatment of 1 relapsing SRP-IMNM case and 2 relapsing dcSSc cases that were highly refractory to the extensive therapeutic interventions, showcasing the efficacy and safety profile of off-the-shelf allogenic CAR-T therapy for refractory autoimmune diseases.

Autoreactive B cells that produce autoantibodies are contributing to the pathogenesis of autoimmunity, for example, anti-SRP for SRP-IMNM and anti-Scl-70 for dcSSc. However, B cell-targeting antibodies like rituximab have achieved only limited success due to incomplete lymphodepletion and residual autoreactive B cells in lymphatic organs or inflamed tissues.[4,24] It is notable that the participant of our trial, S0102, has failed on multiple biologics targeting activated B cells previously, like Belimumab and telitacicept (Table 1), yet responded nicely to our CD19-targeted CAR-T treatment, validating the superiority of CAR-T over B cell depleting antibodies in inducing deep and durable remissions. Additionally, we observed a significant

Figure 5. Safety profile of TyU19 CAR-T therapy in 3 patients

(A) Records of vital signs throughout the treatment and post-treatment follow-up period.

(B) Changes in the absolute cell counts of white blood cells, neutrophils, lymphocytes, platelets, and hemoglobin. The horizontal dashed lines represent the reference range for healthy individuals.

(C) Changes in the absolute cell counts of CD4+ T cells, CD8+ T cells, and NK cells.

(D) Changes in serum level of total immunoglobulin (Ig) G and IgM.

(E) Changes in serum level of C-reactive protein (CRP).

(F) Changes in serum levels of CRS-related cytokines, interleukin (IL)-1β, IL-6, IL-12p70, TNF-α, IFN-α, and IFN-γ. The upper limit of the normal range is depicted by a dashed line in each analyte.

(G) Changes in serum antibodies to EVB, HSVI, HSVII, and CMV.

reduction in B cell infiltration in skin tissue, supporting the efficacy of CD19-targeted CAR-T therapy in depleting B cells both in the bloodstream and in tissues. This observation suggests a mechanism through which tissue fibrosis reversal might be achieved in patients. A pre-conditioning regimen of fludarabine and cyclophosphamide, which are potent lymphodepletion agents, has been applied in these patients, primarily for the purpose of adoptive transfusion of CAR-T cells. Due to the short half-life of chemo (<12 h), lymphocytes would start to recover right after the last dose of chemo, but deep B cell depletion persisted for 2 to 3 months in all 3 patients after CAR-T therapy, and all patients continued to respond for months even after the recovery of all normal lymphocytes including the B cells. In addition, all patients relapsed from prior cyclophosphamide treatment. Therefore, the clinical responses primarily come from the allogeneic CAR-T treatment rather than the non-myeloablative lymphodepleting preconditioning regimens.

Autologous CAR-T therapy targeting B cell markers is highly effective in treating refractory B cell malignancies and in maintaining long-term B cell aplasia.[25] However, long-lasting immune suppression is not desirable in the context of autoimmune patients. An alternative approach, autologous hematopoietic stem cell transplantation (AHSCT), has been used to treat severe cases of SSc, Crohn's disease, and SLE. AHSCT eliminates autoimmune-mediating components and resets the immune balance, achieving long-term remission without requiring continued use of immune suppressants.[26] The successful use of AHSCT suggests that deep, transient depletion of B cells may be sufficient for treating autoimmune patients and achieving durable disease control without the risks of long-term immune suppression. However, the broader application of AHSCT has been limited by its high cost and toxicity.[27]

Although autologous CD19-targeted CAR-T therapies have been recently explored in treating autoimmune diseases and achieved promising efficacy [12–16] preparing autologous CAR-T cells is expensive and time-consuming, putting patients at risk of disease progression and production failures. Allogeneic CAR-T therapy, on the other hand, holds the promise of lowering the cost and logistic barriers of personalized product. A scalable healthy donor-derived, off-the-shelf product would greatly improve the accessibility of CAR-T therapy. Various strategies have been adopted to generate allogeneic product, nevertheless reaching limited success, primarily due to recognition and rejection by adaptive and innate immune responses in the recipients.[17]

Previously, genetic knockout of β2 microglobulin (*B2M*) and class II major histocompatibility class transactivator, *CIITA*, effectively eliminated all HLA class I and class II molecules from the cell surface and thus preventing adaptive immune rejection of the allogeneic transplant.[28] Nevertheless, complete absence of HLA class I molecules led to activation of natural killer (NK) cells.[29] It has been reported that HLA-C, HLA-E, and HLA-G are required to maintain innate immune tolerance,[30–32] while selective disruption of HLA-A and HLA-B molecules effectively improved the immune compatibility of allogeneic induced pluripotent stem cells (iPSCs).[33] Our previous data also demonstrated that the selectively disruption of HLA-A and HLA-B molecules was sufficient to evade T cell-mediated rejection without activating NK cells.[34] Therefore, our strategy involves knocking out T cell receptors by targeting *TRAC* to minimize the risk of GVHD and targeting *HLA-A* and *HLA-B* to reduce rejection by T cells. Other HLA-I genes are preserved to avoid rejection by activated NK cells. In addition, we have knocked out all HLA class II molecules by targeting *CIITA* and *PD-1* to further prolong *in vivo* potency.

In this study, only *HLA-C* locus was demonstrated to be a high-risk off-target site after GUIDE-seq, SITE-seq, and WGS in TyU19 cells. Fortunately, as a classical HLA class I molecule, HLA-C has no direct relationship with T cell transformation, which minimizes the potential genetic risk of TyU19 cells. Furthermore, even though chromosomal fragment inversion, translocation, copy number variation, and large fragment deletion or insertion were all observed in TyU19 cells, the overall quantity of these structural variations was similar with unmodified T cells, indicating that the gene editing did not cause large-scale chromosomal abnormalities. We also observed sequence deletion and insertion along with 1% to 4% of translocation events at different locus in TyU19 cells which is similar with other CRISPR-engineered T cells in clinical use.[35]

As a result, robust expansion of CAR-positive cells was observed in all 3 patients transferred, and CAR-positive cells remained detectable throughout the monitoring period (6 months by the longest follow-up). The treatment achieved deep B cell aplasia lasted for almost 2 months in all 3 patients (Figure 1C). The duration of B cell depletion *in vivo* is comparable to that reported when using autologous CAR-T product.[12–16]

In addition, unlike when using autologous CAR-T product, while our editing strategy has successfully evaded acute immune rejection of the allograft by the host, the allogeneic graft should be eventually rejected due to residual allogeneity. Therefore, the risks for long-term transformation when using allogeneic CAR-T are highly unlikely.[36]

Moreover, the treatment with TyU19 has achieved complete remission in patients with highly refractory and progressive myositis and the reversion of extensive fibrotic damage to critical organs that were traditionally considered irreversible.[8,9] In contrast to conventional management, which depends on continued immune suppression, the responses observed in all 3 patients from this study persisted even after the recovery of normal lymphocytes.

Overall, we have reported promising efficacy and safety profiles of using a scalable, healthy donor-derived, CD19-targeted CAR-T product TyU19 to treat 3 patients with severe autoimmune disorders, which deserve to be validated in broader autoimmune patient population who are refractory to currently available treatments.

Limitations of the study

To explore the potential of a first-in-human universal CAR-T product for the treatment of different patients with distinct types of autoimmune diseases, the study included 1 SRP-IMNM patient and 2 dcSSc patients treated with allogeneic cellular products derived from a single healthy donor. The efficacy and safety of the product will need to be further validated in a larger cohort of patients, and the scalability and robustness of the product will need to be validated in multiple batches derived from different

healthy donors. Although all 3 patients relieved quickly after receiving the treatment and continued to respond even after the recovery of lymphocytes including B cells, we will continue monitoring all patients beyond the reported 6-month period for the long-term efficacy and safety profile. Moreover, only one dose of 1 × 10^6/kg CAR-T product was given to each patient with minimal side effects. Higher dose or multiple dosing may be safely administered and can be explored as needed. Last but not least, we will elaborate on the mechanism of action and the similarities and differences between allogeneic and autologous CAR-T products in our future research.

STAR★METHODS

Detailed methods are provided in the online version of this paper and include the following:

- KEY RESOURCES TABLE
- RESOURCE AVAILABILITY
  - Lead contact
  - Materials availability
  - Data and code availability
- EXPERIMENTAL MODEL AND STUDY PARTICIPANT DETAILS
  - Human participants
- METHOD DETAILS
  - The production, testing, and quality control of allogeneic CAR-T cells
  - Clinical trial information and design
  - Efficacy evaluation
- QUANTIFICATION AND STATISTICAL ANALYSIS
  - Flow cytometry data analysis
  - Processing of whole-genome-sequencing data
  - Bioinformatics analysis of GUIDE-seq and SITE-seq data
  - Bioinformatics analysis of PEM-seq data
  - T1 mapping analysis of CMR imaging
  - Statistical analyses
- ADDITIONAL RESOURCES

SUPPLEMENTAL INFORMATION

Supplemental information can be found online at https://doi.org/10.1016/j.cell.2024.06.027.

ACKNOWLEDGMENTS

X.H. is supported by the National Natural Science Foundation of China (grant no. 82320108010 and 31821003), the National Key Research and Development Project (grant no. 2018AAA0100302), and Shanghai Municipal Key Clinical Specialty (grant no. shslczdzk02602). B.D. is supported by the National Key R&D Program of China (grant no. 2023YFC3402000), the National Natural Science Foundation of China (grant no. 32270960), and the Science and Technology Commission of Shanghai Municipality (23XD1430600). Xiaobing W. is supported by the National Natural Science Foundation of China (grant no. 82271816). Xin W. is supported by the National Natural Science Foundation of China (grant no. 82271852), the National Key R&D Program of China (grant no. 2022YFF1203100), and the Innovative Clinical Research Project of Shanghai Changzheng Hospital, grant/award (grant no. 2020YCXYJ-QN04). Y.Z. is supported by the Pujiang Rheumatism Young Physicians Training Program (grant no. SPROG2212).

AUTHOR CONTRIBUTIONS

Conceptualization: H.X.; methodology: B.D., H.W., B.T., B.Z., J.C., D.L., Y.H., J. Zhang, L.D., and L.S.; investigation: X. Wang, X. Wu, L.Z., Y.X., A.S., S.L. H.Z., W.Y., Y.L., W.L., N.T., L.G., and J.S; resources: H.X. and M.L.; data curation: X. Wang, X. Wu, L.Z., Y.Z., L.L., T.L., J.Y., L.Y., H.L., and X.P.; writing—original draft: X. Wang, X.Wu, and L.Z.; writing—review & editing: H.X., B.D., H.W., M.L., Y.H., J. Zhu, L.D., and L.S.; visualization: J.H., H.C., P.W., J.L., and M.H.; supervision: H.X.; project administration: X. Wang, X. Wu, and L.Z; funding acquisition: H.X., B.D., X. Wang, X. Wu, and Y.Z.; unrestricted access to all data: H.X. and X. Wang.

DECLARATION OF INTERESTS

This study was partially supported by BRL Medicine, Inc.

Received: December 12, 2023
Revised: April 28, 2024
Accepted: June 20, 2024
Published: July 15, 2024

REFERENCES

1. National Institutes of Health; Autoimmune Diseases Coordinating Committee (2005). Autoimmune Diseases Coordinating Committee: Progress in Autoimmune Diseases Research (United States Department of Health and Human Services).
2. Fugger, L., Jensen, L.T., and Rossjohn, J. (2020). Challenges, Progress, and Prospects of Developing Therapies to Treat Autoimmune Diseases. Cell *181*, 63–80. https://doi.org/10.1016/j.cell.2020.03.007.
3. Ma, X., and Bu, B.T. (2022). Anti-SRP immune-mediated necrotizing myopathy: A critical review of current concepts. Front. Immunol. *13*, 1019972. https://doi.org/10.3389/fimmu.2022.1019972.
4. Xiong, A., Yang, G., Song, Z., Xiong, C., Liu, D., Shuai, Y., He, L., Zhang, L., Guo, Z., and Shuai, S. (2021). Rituximab in the treatment of immune-mediated necrotizing myopathy: a review of case reports and case series. Ther. Adv. Neurol. Disord. *14*, 1756286421998918. https://doi.org/10.1177/1756286421998918.
5. Allenbach, Y., Benveniste, O., Stenzel, W., and Boyer, O. (2020). Immune-mediated necrotizing myopathy: clinical features and pathogenesis. Nat. Rev. Rheumatol. *16*, 689–701. https://doi.org/10.1038/s41584-020-00515-9.
6. Gabrielli, A., Avvedimento, E.V., and Krieg, T. (2009). Scleroderma. N. Engl. J. Med. *360*, 1989–2003. https://doi.org/10.1056/NEJMra0806188.
7. LeRoy, E.C., Black, C., Fleischmajer, R., Jablonska, S., Krieg, T., Medsger, T.A., Jr., Rowell, N., and Wollheim, F. (1988). Scleroderma (systemic sclerosis): classification, subsets and pathogenesis. J. Rheumatol. *15*, 202–205.
8. Rubio-Rivas, M., Royo, C., Simeón, C.P., Corbella, X., and Fonollosa, V. (2014). Mortality and survival in systemic sclerosis: systematic review and meta-analysis. Semin. Arthritis Rheum. *44*, 208–219. https://doi.org/10.1016/j.semarthrit.2014.05.010.
9. Kowal-Bielecka, O., Fransen, J., Avouac, J., Becker, M., Kulak, A., Allanore, Y., Distler, O., Clements, P., Cutolo, M., Czirjak, L., et al. (2017). Update of EULAR recommendations for the treatment of systemic sclerosis. Ann. Rheum. Dis. *76*, 1327–1339. https://doi.org/10.1136/annrheumdis-2016-209909.
10. Abbasi, S., Totmaj, M.A., Abbasi, M., Hajazimian, S., Goleij, P., Behroozi, J., Shademan, B., Isazadeh, A., and Baradaran, B. (2023). Chimeric antigen receptor T (CAR-T) cells: novel cell therapy for hematological malignancies. Cancer Med. *12*, 7844–7858. https://doi.org/10.1002/cam4.5551.
11. Ludwig, R.J., Vanhoorelbeke, K., Leypoldt, F., Kaya, Z., Bieber, K., McLachlan, S.M., Komorowski, L., Luo, J., Cabral-Marques, O., Hammers, C.M., et al. (2017). Mechanisms of Autoantibody-Induced Pathology. Front. Immunol. *8*, 603. https://doi.org/10.3389/fimmu.2017.00603.
12. Mougiakakos, D., Krönke, G., Völkl, S., Kretschmann, S., Aigner, M., Kharboutli, S., Böltz, S., Manger, B., Mackensen, A., and Schett, G. (2021). CD19-Targeted CAR T Cells in Refractory Systemic Lupus Erythematosus. N. Engl. J. Med. *385*, 567–569. https://doi.org/10.1056/NEJMc2107725.

13. Pecher, A.C., Hensen, L., Klein, R., Schairer, R., Lutz, K., Atar, D., Seitz, C., Stanger, A., Schneider, J., Braun, C., et al. (2023). CD19-Targeting CAR T Cells for Myositis and Interstitial Lung Disease Associated With Antisynthetase Syndrome. JAMA *329*, 2154–2162. https://doi.org/10.1001/jama.2023.8753.

14. Müller, F., Boeltz, S., Knitza, J., Aigner, M., Völkl, S., Kharboutli, S., Reimann, H., Taubmann, J., Kretschmann, S., Rösler, W., et al. (2023). CD19-targeted CAR T cells in refractory antisynthetase syndrome. Lancet *401*, 815–818. https://doi.org/10.1016/S0140-6736(23)00023-5.

15. Mackensen, A., Müller, F., Mougiakakos, D., Böltz, S., Wilhelm, A., Aigner, M., Völkl, S., Simon, D., Kleyer, A., Munoz, L., et al. (2022). Anti-CD19 CAR T cell therapy for refractory systemic lupus erythematosus. Nat. Med. *28*, 2124–2132. https://doi.org/10.1038/s41591-022-02017-5.

16. Bergmann, C., Müller, F., Distler, J.H.W., Györfi, A.H., Völkl, S., Aigner, M., Kretschmann, S., Reimann, H., Harrer, T., Bayerl, N., et al. (2023). Treatment of a patient with severe systemic sclerosis (SSc) using CD19-targeted CAR T cells. Ann. Rheum. Dis. *82*, 1117–1120. https://doi.org/10.1136/ard-2023-223952.

17. Depil, S., Duchateau, P., Grupp, S.A., Mufti, G., and Poirot, L. (2020). 'Off-the-shelf' allogeneic CAR T cells: development and challenges. Nat. Rev. Drug Discov. *19*, 185–199. https://doi.org/10.1038/s41573-019-0051-2.

18. Aggarwal, R., Rider, L.G., Ruperto, N., Bayat, N., Erman, B., Feldman, B.M., Oddis, C.V., Amato, A.A., Chinoy, H., Cooper, R.G., et al. (2017). 2016 American College of Rheumatology/European League Against Rheumatism criteria for minimal, moderate, and major clinical response in adult dermatomyositis and polymyositis: An International Myositis Assessment and Clinical Studies Group/Paediatric Rheumatology International Trials Organisation Collaborative Initiative. Ann. Rheum. Dis. *76*, 792–801. https://doi.org/10.1136/annrheumdis-2017-211400.

19. Sultan, S.M., Allen, E., Oddis, C.V., Kiely, P., Cooper, R.G., Lundberg, I.E., Vencovsky, J., and Isenberg, D.A. (2008). Reliability and validity of the myositis disease activity assessment tool. Arthritis Rheum. *58*, 3593–3599. https://doi.org/10.1002/art.23963.

20. Khanna, D., Furst, D.E., Clements, P.J., Allanore, Y., Baron, M., Czirjak, L., Distler, O., Foeldvari, I., Kuwana, M., Matucci-Cerinic, M., et al. (2017). Standardization of the modified Rodnan skin score for use in clinical trials of systemic sclerosis. J. Scleroderma Relat. Disord. *2*, 11–18. https://doi.org/10.5301/jsrd.5000231.

21. Khanna, D., Berrocal, V.J., Giannini, E.H., Seibold, J.R., Merkel, P.A., Mayes, M.D., Baron, M., Clements, P.J., Steen, V., Assassi, S., et al. (2016). The American College of Rheumatology Provisional Composite Response Index for Clinical Trials in Early Diffuse Cutaneous Systemic Sclerosis. Arthritis Rheumatol. *68*, 299–311. https://doi.org/10.1002/art.39501.

22. Khanna, D., Huang, S., Lin, C.J.F., and Spino, C. (2021). New composite endpoint in early diffuse cutaneous systemic sclerosis: revisiting the provisional American College of Rheumatology Composite Response Index in Systemic Sclerosis. Ann. Rheum. Dis. *80*, 641–650. https://doi.org/10.1136/annrheumdis-2020-219100.

23. Kolb, M., Peisen, F., Ekert, K., Xenitidis, T., Fritz, J., Ioanoviciu, S.D., Henes, J., and Horger, M. (2021). Shear Wave Elastography for Assessment of Muscular Abnormalities Related to Systemic Sclerosis. Acad. Radiol. *28*, 1118–1124. https://doi.org/10.1016/j.acra.2020.04.043.

24. Kamburova, E.G., Koenen, H.J., Borgman, K.J., ten Berge, I.J., Joosten, I., and Hilbrands, L.B. (2013). A single dose of rituximab does not deplete B cells in secondary lymphoid organs but alters phenotype and function. Am. J. Transplant. *13*, 1503–1511. https://doi.org/10.1111/ajt.12220.

25. Melenhorst, J.J., Chen, G.M., Wang, M., Porter, D.L., Chen, C., Collins, M.A., Gao, P., Bandyopadhyay, S., Sun, H., Zhao, Z., et al. (2022). Decade-long leukaemia remissions with persistence of CD4(+) CAR T cells. Nature *602*, 503–509. https://doi.org/10.1038/s41586-021-04390-6.

26. Alexander, T., and Greco, R. (2022). Hematopoietic stem cell transplantation and cellular therapies for autoimmune diseases: overview and future considerations from the Autoimmune Diseases Working Party (ADWP) of the European Society for Blood and Marrow Transplantation (EBMT). Bone Marrow Transplant. *57*, 1055–1062. https://doi.org/10.1038/s41409-022-01702-w.

27. Pope, J.E., Denton, C.P., Johnson, S.R., Fernandez-Codina, A., Hudson, M., and Nevskaya, T. (2023). State-of-the-art evidence in the treatment of systemic sclerosis. Nat. Rev. Rheumatol. *19*, 212–226. https://doi.org/10.1038/s41584-023-00909-5.

28. Mattapally, S., Pawlik, K.M., Fast, V.G., Zumaquero, E., Lund, F.E., Randall, T.D., Townes, T.M., and Zhang, J. (2018). Human Leukocyte Antigen Class I and II Knockout Human Induced Pluripotent Stem Cell-Derived Cells: Universal Donor for Cell Therapy. J. Am. Heart Assoc. *7*, e010239. https://doi.org/10.1161/JAHA.118.010239.

29. Long, E.O., Kim, H.S., Liu, D., Peterson, M.E., and Rajagopalan, S. (2013). Controlling natural killer cell responses: integration of signals for activation and inhibition. Annu. Rev. Immunol. *31*, 227–258. https://doi.org/10.1146/annurev-immunol-020711-075005.

30. Hong, C.H., Sohn, H.J., Lee, H.J., Cho, H.I., and Kim, T.G. (2017). Antigen Presentation by Individually Transferred HLA Class I Genes in HLA-A, HLA-B, HLA-C Null Human Cell Line Generated Using the Multiplex CRISPR-Cas9 System. J. Immunother. *40*, 201–210. https://doi.org/10.1097/CJI.0000000000000176.

31. Ferreira, L.M.R., Meissner, T.B., Tilburgs, T., and Strominger, J.L. (2017). HLA-G: At the Interface of Maternal-Fetal Tolerance. Trends Immunol. *38*, 272–286. https://doi.org/10.1016/j.it.2017.01.009.

32. Lee, N., Llano, M., Carretero, M., Ishitani, A., Navarro, F., López-Botet, M., and Geraghty, D.E. (1998). HLA-E is a major ligand for the natural killer inhibitory receptor CD94/NKG2A. Proc. Natl. Acad. Sci. USA *95*, 5199–5204. https://doi.org/10.1073/pnas.95.9.5199.

33. Xu, H., Wang, B., Ono, M., Kagita, A., Fujii, K., Sasakawa, N., Ueda, T., Gee, P., Nishikawa, M., Nomura, M., et al. (2019). Targeted Disruption of HLA Genes via CRISPR-Cas9 Generates iPSCs with Enhanced Immune Compatibility. Cell Stem Cell *24*, 566–578.e7. https://doi.org/10.1016/j.stem.2019.02.005.

34. Chen, X., Tan, B., Xing, H., Zhao, X., Ping, Y., Zhang, Z., Huang, J., Shi, X., Zhang, N., Lin, B., et al. (2024). Allogeneic CAR-T cells with of HLA-A/B and TRAC disruption exhibit promising antitumor capacity against B cell malignancies. Cancer Immunol. Immunother. *73*, 13. https://doi.org/10.1007/s00262-023-03586-1.

35. Stadtmauer, E.A., Fraietta, J.A., Davis, M.M., Cohen, A.D., Weber, K.L., Lancaster, E., Mangan, P.A., Kulikovskaya, I., Gupta, M., Chen, F., et al. (2020). CRISPR-engineered T cells in patients with refractory cancer. Science *367*, eaba7365. https://doi.org/10.1126/science.aba7365.

36. Verdun, N., and Marks, P. (2024). Secondary Cancers after Chimeric Antigen Receptor T-Cell Therapy. N. Engl. J. Med. *390*, 584–586. https://doi.org/10.1056/NEJMp2400209.

37. Bae, S., Park, J., and Kim, J.S. (2014). Cas-OFFinder: a fast and versatile algorithm that searches for potential off-target sites of Cas9 RNA-guided endonucleases. Bioinformatics *30*, 1473–1475. https://doi.org/10.1093/bioinformatics/btu048.

38. Chen, S., Zhou, Y., Chen, Y., and Gu, J. (2018). fastp: an ultra-fast all-in-one FASTQ preprocessor. Bioinformatics *34*, i884–i890. https://doi.org/10.1093/bioinformatics/bty560.

39. Li, H., and Durbin, R. (2009). Fast and accurate short read alignment with Burrows-Wheeler transform. Bioinformatics *25*, 1754–1760. https://doi.org/10.1093/bioinformatics/btp324.

40. Li, H., Handsaker, B., Wysoker, A., Fennell, T., Ruan, J., Homer, N., Marth, G., Abecasis, G., and Durbin, R.; 1000 Genome Project Data Processing Subgroup (2009). The Sequence Alignment/Map format and SAMtools. Bioinformatics *25*, 2078–2079. https://doi.org/10.1093/bioinformatics/btp352.

41. Van der Auwera, G.A., and O'Connor, B.D. (2020). Genomics in the Cloud: Using Docker, GATK, and WDL in Terra, First Edition (O'Reilly Media).

42. Broad Institute (2019). Picard toolkit. GitHub. https://broadinstitute.github.io/picard/.

43. Wang, K., Li, M., and Hakonarson, H. (2010). ANNOVAR: functional annotation of genetic variants from high-throughput sequencing data. Nucleic Acids Res. *38*, e164. https://doi.org/10.1093/nar/gkq603.

44. Talevich, E., Shain, A.H., Botton, T., and Bastian, B.C. (2016). CNVkit: Genome-Wide Copy Number Detection and Visualization from Targeted DNA Sequencing. PLoS Comput. Biol. *12*, e1004873. https://doi.org/10.1371/journal.pcbi.1004873.

45. Layer, R.M., Chiang, C., Quinlan, A.R., and Hall, I.M. (2014). LUMPY: a probabilistic framework for structural variant discovery. Genome Biol. *15*, R84. https://doi.org/10.1186/gb-2014-15-6-r84.

46. Chen, T., Chen, X., Zhang, S., Zhu, J., Tang, B., Wang, A., Dong, L., Zhang, Z., Yu, C., Sun, Y., et al. (2021). The Genome Sequence Archive Family: Toward Explosive Data Growth and Diverse Data Types. Genomics Proteomics Bioinformatics *19*, 578–583. https://doi.org/10.1016/j.gpb.2021.08.001.

47. CNCB-NGDC Members and Partners (2024). Database Resources of the National Genomics Data Center, China National Center for Bioinformation in 2024. Nucleic Acids Res. *52*, D18–D32. https://doi.org/10.1093/nar/gkad1078.

48. Tsai, S.Q., Zheng, Z., Nguyen, N.T., Liebers, M., Topkar, V.V., Thapar, V., Wyvekens, N., Khayter, C., Iafrate, A.J., Le, L.P., et al. (2015). GUIDE-seq enables genome-wide profiling of off-target cleavage by CRISPR-Cas nucleases. Nat. Biotechnol. *33*, 187–197. https://doi.org/10.1038/nbt.3117.

49. Cameron, P., Fuller, C.K., Donohoue, P.D., Jones, B.N., Thompson, M.S., Carter, M.M., Gradia, S., Vidal, B., Garner, E., Slorach, E.M., et al. (2017). Mapping the genomic landscape of CRISPR-Cas9 cleavage. Nat. Methods *14*, 600–606. https://doi.org/10.1038/Nmeth.4284.

50. Yin, J., Liu, M., Liu, Y., Wu, J., Gan, T., Zhang, W., Li, Y., Zhou, Y., and Hu, J. (2019). Optimizing genome editing strategy by primer-extension-mediated sequencing. Cell Discov. *5*, 18. https://doi.org/10.1038/s41421-019-0088-8.

51. Lundberg, I.E., Tjärnlund, A., Bottai, M., Werth, V.P., Pilkington, C., de Visser, M., Alfredsson, L., Amato, A.A., Barohn, R.J., Liang, M.H., et al. (2017). 2017 European League Against Rheumatism/American College of Rheumatology Classification Criteria for Adult and Juvenile Idiopathic Inflammatory Myopathies and Their Major Subgroups. Arthritis Rheumatol. *69*, 2271–2282. https://doi.org/10.1002/art.40320.

52. Sorensen, M.D., Harper, J.D., Borofsky, M.S., Hameed, T.A., Smoot, K.J., Burke, B.H., Levchak, B.J., Williams, J.C., Bailey, M.R., Liu, Z., et al. (2022). Removal of Small, Asymptomatic Kidney Stones and Incidence of Relapse. N. Engl. J. Med. *387*, 506–513. https://doi.org/10.1056/NEJMoa2204253.

53. de Prost, N., Pham, T., Carteaux, G., Mekontso Dessap, A., Brun-Buisson, C., Fan, E., Bellani, G., Laffey, J., Mercat, A., Brochard, L., and Maître, B. (2017). Etiologies, diagnostic work-up and outcomes of acute respiratory distress syndrome with no common risk factor: a prospective multicenter study. Ann. Intensive Care *7*, 69. https://doi.org/10.1186/s13613-017-0281-6.

54. van den Hoogen, F., Khanna, D., Fransen, J., Johnson, S.R., Baron, M., Tyndall, A., Matucci-Cerinic, M., Naden, R.P., Medsger, T.A., Jr., Carreira, P.E., et al. (2013). 2013 classification criteria for systemic sclerosis: an American college of rheumatology/European league against rheumatism collaborative initiative. Ann. Rheum. Dis. *72*, 1747–1755. https://doi.org/10.1136/annrheumdis-2013-204424.

55. Goldin, J., Elashoff, R., Kim, H.J., Yan, X., Lynch, D., Strollo, D., Roth, M.D., Clements, P., Furst, D.E., Khanna, D., et al. (2009). Treatment of scleroderma-interstitial lung disease with cyclophosphamide is associated with less progressive fibrosis on serial thoracic high-resolution CT scan than placebo: findings from the scleroderma lung study. Chest *136*, 1333–1340. https://doi.org/10.1378/chest.09-0108.

56. Maurer, B., Graf, N., Michel, B.A., Müller-Ladner, U., Czirják, L., Denton, C.P., Tyndall, A., Metzig, C., Lanius, V., Khanna, D., and Distler, O. (2015). Prediction of worsening of skin fibrosis in patients with diffuse cutaneous systemic sclerosis using the EUSTAR database. Ann. Rheum. Dis. *74*, 1124–1131. https://doi.org/10.1136/annrheumdis-2014-205226.

57. Burt, R.K., Shah, S.J., Dill, K., Grant, T., Gheorghiade, M., Schroeder, J., Craig, R., Hirano, I., Marshall, K., Ruderman, E., et al. (2011). Autologous non-myeloablative haemopoietic stem-cell transplantation compared with pulse cyclophosphamide once per month for systemic sclerosis (ASSIST): an open-label, randomised phase 2 trial. Lancet *378*, 498–506. https://doi.org/10.1016/S0140-6736(11)60982-3.

58. Goh, N.S., Hoyles, R.K., Denton, C.P., Hansell, D.M., Renzoni, E.A., Maher, T.M., Nicholson, A.G., and Wells, A.U. (2017). Short-Term Pulmonary Function Trends Are Predictive of Mortality in Interstitial Lung Disease Associated With Systemic Sclerosis. Arthritis Rheumatol. *69*, 1670–1678. https://doi.org/10.1002/art.40130.

59. Cerqueira, M.D., Weissman, N.J., Dilsizian, V., Jacobs, A.K., Kaul, S., Laskey, W.K., Pennell, D.J., Rumberger, J.A., Ryan, T., and Verani, M.S.; American Heart Association Writing Group on Myocardial Segmentation and Registration for Cardiac Imaging (2002). Standardized myocardial segmentation and nomenclature for tomographic imaging of the heart. A statement for healthcare professionals from the Cardiac Imaging Committee of the Council on Clinical Cardiology of the American Heart Association. Circulation *105*, 539–542. https://doi.org/10.1161/hc0402.102975.

STAR★METHODS

KEY RESOURCES TABLE

REAGENT or RESOURCE	SOURCE	IDENTIFIER
Antibodies		
FITC Mouse Anti-Human CD19	ACRObiosystems	Cat#CD9-HF2H2 and CD9-HF251 RRID: AB_3076267 and AB_3076268
APC Anti-Human CD3	Biolegend	Cat#300312 RRID: AB_314048
PE Mouse Monoclonal Anti-Human HLA-A	BD biosciences	Cat#567739 RRID: AB_2916718
BB700 Rat Monoclonal Anti-Human HLA-B	BD biosciences	Cat#752626 RRID: AB_2917612
PE-Cy7 Mouse Monoclonal Anti-Human HLA-DR	BD biosciences	Cat#560651 RRID: AB_1727528
BV421 Mouse Monoclonal Anti-Human CD279 (PD-1)	BD biosciences	Cat#562516 RRID: AB_11153482
Rabbit Polyclonal Anti-TGF beta 1	Abclone	Cat#A2124 RRID: AB_2764143
Mouse Monoclonal Anti-CK5/6	ZSGB-BIO	Cat#ZM-0313 RRID: AB_3076263
Rabbit Monoclonal Anti-SRP54	Abcam	Cat#ab154796 RRID: AB_3076262
Rabbit Monoclonal Anti-CD4	ZSGB-BIO	Cat#ZA-0519 RRID: AB_3076264
Rabbit Monoclonal Anti-CD8	ZSGB-BIO	Cat#ZA-0508 RRID: AB_2890107
Mouse Monoclonal Anti-CD68	ZSGB-BIO	Cat#ZM-0464 RRID: AB_3076266
Mouse Monoclonal Anti-CD19	ZSGB-BIO	Cat# ZM-0038 RRID: AB_3096421
Chemicals, peptides, and recombinant proteins		
CAR containing plasmid	BioVector NTCC	Cat#pELPs 19-BB-z
pELPs	Addgene	Cat#193253
pRSV-Rev	Addgene	Cat#12253
pMDLg/pRRE (Gag/Pol)	Addgene	Cat#12251
pMD2.G (VSVG envelope) packaging plasmid DNA	Addgene	Cat#12259
polyethyleneimine (PEI)	MCE	Cat#HY-K2014
X-VIVO 15 medium	LONZA	Cat#02-053Q
Sp.Cas9 protein	Thermofisher	Cat#A36499
sgRNA	GenScript	Customized
p3s-Cas9HC	Add gene	Cat#43945
Proteinase K	TransGen Biotech	Cat#GE201-01
RNase A	TransGen Biotech	Cat#GE101-01
Dynabeads MyOne Streptavidin T1 beads	Invitrogen	Cat#65601
Critical commercial assays		
TruSeq Nano DNA LT Sample Prepararion kit	Illumina	Cat#FC-121-4001
P3 Primary Cell 4D-Nucleofector X Kit S	LONZA	Cat#V4XP-3032
Cytokine Co-Detection Kit (Immunofluorescence)	CELLGENE BIO	Cat#P110100403
KAPA HTP Library Preparation Kit	KAPA BIOSYSTEMS	Cat#KR0426
Deposited data		
Raw data of whole-genome sequencing (WGS), GUIDE-Seq, SITE-Seq and primer extension-mediated sequencing (PEM-seq)	HRA007533	https://bigd.big.ac.cn/gsa-human/browse/HRA007533
Experimental models: Cell lines		
Human embryonic kidney 293T cells	ATCC	CRL-3216
Software and algorithms		
Cas-OFFinder	CRISPR RGEN Tools[37]	http://www.rgenome.net
Illumina HiSeq X Ten platform	Qingdao OE Biotech	https://www.illumina.com.cn/systems/sequencing-platforms.html
PANNORAMIC MIDI II	3DHISTECH Ltd	https://www.3dhistech.com/research/pannoramic-digital-slide-scanners/pannoramic-midi/

(*Continued on next page*)

Continued		
REAGENT or RESOURCE	SOURCE	IDENTIFIER
fastp	Chen et al.[38]	https://github.com/OpenGene/fastp
BWA V0.7.12	Li et al.[39]	https://bio-bwa.sourceforge.net/
SAMtools V1.4	Li et al.[40]	http://www.htslib.org/download/
GATK V4.1.0.0	Broad Institute[41]	https://gatk.broadinstitute.org/hc/en-us
Picard V4.1.0.0	Broad Institute[42]	https://broadinstitute.github.io/picard/
ANNOVAR	Talevich et al.[43]	https://annovar.openbioinformatics.org/en/latest/
CNVkit V 0.9.5	Layer et al.[44]	http://cnvkit.readthedocs.io/
Lumpy V0.2.13	Tsai et al.[45]	https://github.com/arq5x/lumpy-sv
Other		
FACSCalibur system	BD biosciences	https://www.bdbiosciences.com/zh-cn
Electroporation systems	MaxCyte	https://maxcyte.com/
Bioruptor pico	Diagenode	https://www.diagenode.com/en/p/bioruptor-pico-sonication-device
Aixplorer US system	SuperSonic Imagine	https://www.supersonicimagine.com/cn/Aixplorer-R/node_117

RESOURCE AVAILABILITY

Lead contact

Further information and requests for resources should be directed to and will be fulfilled by the lead contact, Huji Xu (xuhuji@smmu.edu.cn).

Materials availability

This study did not generate new reagents.

Data and code availability

- The raw data of WGS, GUIDE-Seq, SITE-Seq and PEM-seq reported in this paper have been deposited in the Genome Sequence Archive[46] in National Genomics Data Center,[47] China National Center for Bioinformation/Beijing Institute of Genomics, Chinese Academy of Sciences (GSA-Human: HRA007533) that are publicly accessible at https://ngdc.cncb.ac.cn/gsa-human. Accession numbers are listed in the key resources table.
- This paper does not report original code.
- Any additional information required to reanalyze the data reported in this paper is available from the lead contact upon request.

EXPERIMENTAL MODEL AND STUDY PARTICIPANT DETAILS

Human participants

Healthy donor for TyU19 CAR-T Cell Manufacturing

The study involved a single 21-year-old Asian woman for TyU19 CAR-T cell manufacturing, who was strictly screened according to the ethical and safety procedures approved by the Clinical Ethics Committee of the First Affiliated Hospital, College of Medicine, Zhejiang University (Ethics Approval Number: IIT20210001C-R1 for human subjects).

Patients with refractory autoimmune diseases involved in TyU19 CAR-T therapy

The study involved three patients with refractory autoimmune diseases: two males (ages 45 and 56) diagnosed with systemic sclerosis (SSc) and one female (age 42) diagnosed with immune-mediated necrotizing myopathy (IMNM). All patients were from southeast China. The patients were strictly screened according to inclusion and exclusion criteria (mentioned in "Clinical trial information and design"). The demographic characteristics, baseline clinical characteristics, and previous treatment history of the patients are shown in Table 1.

METHOD DETAILS

The production, testing, and quality control of allogeneic CAR-T cells

Construction of CAR cassette

Second-generation CD19 CAR were constructed using single chain antibody fragments derived from antibody clones FMC63, hinge and transmembrane regions from CD8A, intracellular domain from 4-1BB (CD137), and intracellular domain from CD3-zeta subunit

(pELPs 19-BB-z). CD19 CAR and extracellular domain of PD-L1 (PD-L1 ECD) were cloned into a commercial lentiviral vector backbone pELPS downstream from an EF1a promoter and were flanked by lenti-viral 5′ and 3′ long-terminal repeats (LTRs).

Lentiviral package and transduction

Third-generation, self-inactivating lentiviral supernatant was produced in the 293T cells. In brief, 70% confluent 293T 10cm plates were co-transfected with 10 μg pELPS vector plasmid, and 4 μg pRSV-Rev, 4 μg pMDLg/pRRE (Gag/Pol) and 6 μg pMD2.G (VSVG envelope) packaging plasmid DNA using polyethyleneimine (PEI). Medium was replaced at 24 h after transfection. The 72-h viral supernatants were collected, combined, and concentrated by ultracentrifugation at 25,000 rpm for 2.5 h. Concentrated lentiviral stocks were frozen with X-VIVO 15 medium (LONZA) at −80 °C for future use. For lentiviral infection, cells were co-cultured with CD19-CAR cassette containing lentivirus vector for 72h (37°C, 5% CO2) with the multiplicity of infection (MOI) of 8. After the infection, cells were washed twice with wash buffer, and then prepared for nucleofection with MaxCyte electroporation systems.

CRISPR knockout

CRISPR-Cas9 gene knockout was performed by transient Cas9/gRNA (RNP) complex electroporation using the MaxCyte electroporation systems (MaxCyte). On day 5 of culture, CAR T cells were counted, pelleted, and resuspended in electroporation buffer at 1×10^8 cells per 1 ml reaction. 70μg Sp. Cas9 protein (Thermofisher) and 70μg chemically modified synthetic sgRNA (GenScript, China) (1:1 mass ratio gRNA:Cas9) per reaction was pre-complexed for 20 min at room temperature to create ribonucleoprotein complexes (RNP). A 1 ml cell suspension was mixed with RNP and electroporated using the ‘‘Expanded T cell 2’’ program in the electroporation cassette (CL-1.1). Cells were recovered at 37°C for 20 min in 1 ml T cell medium (X-VIVO15, LONZA) then expanded as usual. Knockout efficiency was determined using fluorescence-activated cell sorting (FACS) on day5 after the electroporation.

Off-target assessment

We used Cas-OFFinder (http://www.rgenome.net) to find potential off-target sites that differed from on-target sequences by up to 8 nt mismatches. For whole-genome-sequencing, genomic DNA was extracted using standard protocols. TruSeq Nano DNA LT Sample Prepararion kit (Illumina, San Diego, CA, USA) was used for DNA libraries. The libraries were subjected to massively parallel sequencing in the Illumina HiSeq X Ten platform (Qingdao OE Biotech, China) to generate 150bp paried-end reads. Data analysis was also conducted by OE Biotech Co., Ltd (Qingdao, China). For WGS bioinformatics, raw reads were filtered using fastp (Version 0.19.5). Clean reads were aligned to the reference human genome (GRCh37) using BWA (version 0.7.12), after which the mapped reads were sorted and indexed with SAMtools (Version 1.4). To generate analysis-ready BAM files, recalibration of base quality scores, single nucleotide polymorphism (SNP) and insertion/deletion (INDEL) realignment were performed using GATK (Version 4.1.0.0), while duplicate reads were marked using Picard (Version 4.1.0.0). Variant calling was conducted using these final BAM files, with reference to several annotation databases such as Refseq, 1000 Genomes, the Catalogue of Somatic Mutations in Cancer (COSMIC), OMIM, etc. ANNOVAR was used for annotation. Copy number variation (CNV) was inferred from sequencing data using CNVkit (Version 0.9.5), while structural variation (SV) was called using Lumpy software (Version 0.2.13). The resulting genomic variation information was visualized using a Circos diagram. GUIDE-Seq and SITE-Seq were conducted as described in references Tsai et al.[48] and Cameron et al.[49] In brief, for GUIDE-seq library construction, 2×10^5 activated T cells were transfected with plasmids expressing sgRNA (500 ng, pAAV-Albumin or pAAV-PCSK9) and Cas9 (500 ng, p3s-Cas9HC; Addgene plasmid #43945) and 5 pmol dsODN using LONZA P3 electroporation kit (V4XP-3032; program EN-158). Transfected cells were transferred to a 24-well plate containing X-VIVO15 completed medium (1 ml/well) that had been pre-incubated at 37°C and cultured for 2 days. Genomic DNA was extracted and randomly fragmented to 500bp by Bioruptor pico (Diagenode) ultra-sonication. Adapters were ligated to the end-repaired DNA, and then two rounds of PCR were performed to amplify the sequence carrying dsODN tag. The library was sequenced on MGI 2000 platform with 150-bp paired-end reads. Data was analyzed using open-source GUIDE-seq software (http://jounglab.org/guideseq). For SITE-Seq preparation, high molecular weight (HMW) genomic DNA (gDNA) was purified from activated T cells. Then, 7.5 μg HMW gDNA was subjected to in vitro digestion with 64 nM SpCas9 and 256 nM sgRNA. After terminated by Proteinase K (TransGen Biotech) and RNase A (TransGen Biotech), the digested products were end-repaired, A-tailed and ligated to the annealed adaptor set 1. The adaptor-ligated DNA was then fragmented by NEBNext dsDNA Fragmentase (NEB) and then quenched with 0.5 M EDTA. The fragmented DNA was then ligated to the second adaptor by KAPA HTP library preparation kit (KAPA BIOSYSTEMS). Then, the dual adaptor-ligated DNA was enriched with Dynabeads MyOne Streptavidin T1 beads (Invitrogen). Finally, two rounds of nested PCR amplification to recovery DNA from streptavidin beads and to add index for sequencing. Completed libraries were quantified and sequenced on MGI 2000 platform with 150-bp paired-end reads.

Primer extension-mediated sequencing

Each PEM-seq DNA library was constructed according to the standard procedure,[50] for which 20 μg of genomic DNA from different Cas nuclease-edited samples is generally required. The control sample of each target site was generally applied to the genome of wild-type cells. For the PEM-seq procedure, first, the genomic DNA was sonicated with a Bioruptor pico (Diagenode) ultra-sonication to obtain 300-700 bp DNA fragments. Then, a biotinylated primer was designed within 150 bp from the target site to accomplish primer extension. Biotinylated single-stranded DNA was enriched with Dynabeads™ MyOne™ Streptavidin T1 (Thermo Fisher) and ligated with a ‘‘bridge adaptor’’, which was designed to achieve exponential amplification of the target fragments. On-bead nested PCR was performed with specific primes followed by size selection and amplification. Finally, the DNA libraries were sequenced on an MGI2000 platform. Deletion refers to the deletion of a length from 1 bp to 100 bp at the cut site. Insertion refers to the insertion of a length from 1 bp to 100 bp at the cut site. Translocation includes intra translations from deletions, intra translations from inversion, and inter translations. Intra translations from deletions are sequences located at a distance of over 500kb from the cut

site and translocated downstream of the cut site. Intra translocations from inversion are sequences located at a distance of over 500kb from the cut site translocated upstream of the cut site. Inter translocations are chromosomal translocations at the cut site.

Flow cytometry for cell analysis

CAR was labelled with FITC-conjugated human CD19 (20-291) protein (ACRO biosystems, CD9-HF2H2 and CD9-HF251). For T cell phenotyping the following antibodies were used: APC anti-human CD3 (300312) was from Biolegend; PE Mouse Anti-Human HLA-A (567739), BB700 Rat anti-human HLA-B (752626), PE Cy7 mouse anti-human HLA-DR (560651) and BV421 mouse anti-human CD279 (PD-1) (562516) were from BD biosciences.

Clinical trial information and design

This was an investigator-initiated study designed to evaluate the safety and efficacy of allogeneic anti-CD19 CAR-T cells in treating refractory autoimmune disease. The clinical protocol has been registered at ClinicalTrials.gov (NCT05859997).

Common inclusion criteria

1) Age ranges from 18 to 65 years old (including threshold), regardless of gender.
2) Positive expression of CD19 on peripheral blood B cells determined by flow cytometry.
3) The functions of important organs meet the following requirements:
   A Bone marrow function needs to meet: a. White blood cell count $\geq 3\times 10^9$/L; b. Neutrophil count $\geq 1\times10^9$/L (no colony-stimulating factor treatment within 2 weeks before examination); c. Hemoglobin$\geq$ 60g/L.
   B Liver function: ALT $\leq 3\times$ULN, AST$\leq 3\times$ULN, TBIL$\leq 1.5\times$ULN (excluding Gilbert syndrome, total bilirubin $\leq 3.0\times$ULN) (No requirements for conditions caused by the disease itself).
   C Renal function: creatinine clearance rate (CrCl) $\geq$ 60 ml/minute (Cockcroft/Fault formula).
   D Coagulation function: International standardized ratio (INR) $< 1.5\times$ULN, prothrombin time (PT) $< 1.5\times$ULN.
   E Cardiac function: Good hemodynamic stability.
4) Female subjects with fertility and male subjects whose partners are women of childbearing age are required to use medically approved contraception or abstinence during the study treatment period and at least 6 months after the end of the study treatment period; Female subjects of childbearing age tested negative for serum HCG within 7 days before enrollment in the study and were not in lactation.
5) Voluntarily participate in this clinical study, sign an informed consent form, have good compliance, and cooperate with follow-up.

The specific inclusion criteria for inflammatory myositis

1) Diagnosis with the 2017 EULAR/ACR classification criteria for inflammatory myopathies (including DM, PM, ASS and NM).[51]
2) For those with muscle involvement, the MMT-8 score is lower than 142 and there are at least two abnormal findings in the following five core measurements (PhGA, PtGA or extramuscular disease activity score $\geq$ 2 points; HAQ total score $\geq$ 0.25; muscle enzymes The level is 1.5 times the upper limit of the normal range).[52]
3) Myositis antibody positive.
4) Needs to be met A or B:
   A Patients with relapse and refractory myopathy: Conventional treatment is ineffective, or disease activity reappears after remission. The definition of routine treatment: the use of glucocorticoids (more than 1 mg/Kg/d) and cyclophosphamide, and any one or more of the following immunomodulatory drugs for more than 6 months: antimalarial drugs, azathioprine, mycophenolate mofetil, methotrexate, leflunomide, tacrolimus, cyclosporine, and biological agents including rituximab, belimumab, telitacicept, etc.
   B Patients with progressive disorder: Rapidly progressive interstitial pneumonia occurring within a short period of time.[53]

The specific inclusion criteria for systemic sclerosis

1) Conformity with the 2013 American College of Rheumatology (ACR) classification criteria for scleroderma,[54] exhibiting diffuse cutaneous manifestations (skin thickening proximal to the elbows or knees and/or torso, in addition to distal extremity involvement).
2) Concurrent active interstitial lung disease (ILD): indicated by ground-glass opacities on High-Resolution Computed Tomography (HRCT)[55] and pulmonary function tests showing Forced Vital Capacity (FVC) or Diffusing Capacity for Carbon Monoxide (DLCO) less than 70% of the predicted value.
3) Needs to be met A or B:
   A Classification as refractory or relapsed cases unresponsive to standard treatment or recurrence of disease activity post-remission. Standard treatment is defined as the use of glucocorticoids (at a dosage exceeding 0.5 mg/Kg/d) and cyclophosphamide, along with any of the following immunomodulatory medications for more than six months: antimalarials, azathioprine, mycophenolate mofetil, methotrexate, leflunomide, tacrolimus, cyclosporine, and biologics including rituximab, belimumab, tocilizumab, etc.
   B Presence of progressive disease, specifically defined as: a) Progression of skin involvement: an increase in the modified Rodnan Skin Score (mRSS) by more than 25%[56,57]; b) Progression of lung disease: a reduction in FVC by 10%,

or a reduction in FVC by 5% accompanied by a 15% decrease in DLCO.[58]

4 Common exclusion criteria:
   1) Individuals with a history of severe drug allergies or allergic constitution.
   2) Existence or suspicion of uncontrollable or treatable fungal, bacterial, viral or other infections.
   3) Individuals with relatively serious heart diseases, such as angina pectoris, myocardial infarction, heart failure, and arrhythmia.

4)Subjects with congenital immunoglobulin deficiency.

5) Other malignant tumors (excluding non-melanoma skin cancer, cervical cancer *in situ*, bladder cancer, and breast cancer that have survived for more than 5 years without disease).

6) Subjects with end-stage renal failure.

7) Subjects with positive hepatitis B B surface antigen (HBsAg) or hepatitis B core antibody (HBcAb) and HBV DNA titer in peripheral blood higher than the upper limit of detection; Patients with positive hepatitis C virus (HCV) antibodies and positive peripheral blood HCV RNA; People who are positive for human immunodeficiency virus (HIV) antibodies; Those who have tested positive for syphilis.

8) Having mental illness and severe cognitive impairment.

9) Those who have participated in other clinical trials within the first 3 months of enrollment.

10) Pregnant or intending to conceive women.

11) The researchers believe that there are other reasons why subjects cannot be included in this study.

Specific exclusion criteria for inflammatory myositis

1) Drug-induced myopathy.
2) Inclusion body myositis.
3) Tumor-related myositis (myositis occurring within 2 years after the diagnosis of tumor).

Specific exclusion criteria for systemic sclerosis

1) New York Heart Association (NYHA) functional class IV.
2) Significant abnormalities on High-Resolution Computed Tomography (HRCT) not caused by systemic sclerosis.
3) Persistent unexplained hematuria (more than 5 red blood cells under high power field) or creatinine clearance rate <40 ml/min.
4) Signs of renal crisis.
5) Active gastric antral vascular ectasia.

Ethics approval

The trial was approved by the institutional review board, and all patients provided written informed consent in accordance with the Declaration of Helsinki before enrolment. The clinical protocol was reviewed and approved by the Clinical Research Ethics Committee of ShangHai Changzheng Hospital (Ethics Approval Number: 2023SL010).

Therapy and follow-up

1) Preconditioning strategy: Prior to the administration of the TyU19 infusion, all immunosuppressive medications were discontinued, except for glucocorticoids, which were tapered to a dose deemed appropriate by the treating physicians.
2) Conditioning regimen: Patients received 25 mg/m^2/day Fludarabine (FLU) from day -5 to day -3, and 300 mg/m^2/day Cyclophosphamide (CTX) on days -5 and -4.
3) Patients received an intravenous infusion of CAR T cells at a dose of 1×10^6 cells/kg on D0.
4) Post-therapy cell proliferation was examined on D0, D2, D4, D7±1d, D10±2d, D14±2d, D21±2d, D30±3d, M2±3d, M3±3d, M6±7d, M9±7d, M12±7d.
5) Clinical outcomes were methodically evaluated at specific intervals: baseline, Day 14 ± 2 days, Day 21 ± 2 days, Day 30 ± 3 days, Month 2 ± 3 days, Month 3 ± 3 days, Month 6 ± 7 days, Month 9 ± 7 days, and Month 12 ± 7 days, accompanied by thorough monitoring for potential adverse events.

Efficacy evaluation

Efficacy evaluation for inflammatory myositis

1) The major clinical improvement from the baseline was evaluated by Total Improvement Score (TIS).[18] The scale of efficacy was defined as minimal (≥ 20), moderate (≥ 40), and major (≥ 60).
2) Other clinical improvement assessments included evaluation of disease activity in extramuscular organs by the Myositis Disease Activity Assessment Tool (MDAAT), an overall assessment of extramuscular involved organs, including MYOACT and MITAX.[19]
3) Muscle inflammatory infiltration was measured by MRI imaging. This measurement was performed by sophisticated radiologists from Department of Radiology, Changzheng Hospital, Naval Medical University.
4) The level of anti-SRP autoantibody by quantitative immunoblotting analysis. The analysis was conducted at Hangzhou Dian Medical Laboratory Center, and the reagent kits were supplied by EUROIMMUN. BlueDiver Dot Myositis12 SAE IgG is

an Immunodot kit used for the detection in human sera of IgG autoantibodies against SRP and performed on the BlueDiver Instrument (hereafter BDI). The test is based on the principle of an Enzyme Immunoassay. Briefly: the strips are first incubated with diluted patients' sera. Upon further incubation into AP-conjugated goat antibodies against human IgG after washing, the enzyme conjugate binds to the antigen-antibody complexes. After removal of excess conjugate by washing, the strips are finally incubated into a substrate solution. Enzyme activity, if present, leads to the development of purple dots on the membrane pads. The intensity of the coloration is directly proportional to the amount of antibody present in the sample.

5) Pathological changes and immune infiltration in thigh muscle were determined by hematoxylin and eosin staining and immunohistochemistry before TyU19 therapy, on M2, M3 and M6. Muscle biopsies were performed at each time point from the lateral side of the right thigh of the patient using ultrasound-guided thick needle aspiration method. The muscle tissue was fixed in 4% paraformaldehyde and then processed for paraffin embedding. The tissue sections were stained with hematoxylin and eosin for histopathological examination. Nuclei are stained a distinct blue with Hematoxylin, while the cytoplasm is stained varying shades of pink to peach with Eosin. Immunohistochemistry was employed to detect the infiltration of SRP and immune-inflammatory cells. This was achieved using an SRP antibody (Abcam, ab154796) at a dilution of 1:200, CD4 antibody (ZSGB-BIO, ZA-0519), CD8 antibody (ZSGB-BIO, ZA-0508) at a dilution of 1:200 and CD68 antibody (ZSGB-BIO, ZM0464).

Efficacy evaluation for systemic sclerosis

1) The major clinical improvement from the baseline was evaluated by the ACR-CRISS score which is a weighted score consisting of 5 domains, including modified Rodnan skin score (mRSS),[20] Health Assessment Questionnaire Index (HAQ-DI), forced vital capacity (FVC) by pneumonia function test, and patient and physician global assessments (VAS score, 0-10). ACR-CRISS score of $\geq$ 0.6 is considered an improvement, while a score of < 0.6 indicates no improvement.[21] The revised CRISS score was assessed for each patient at each time point.[22] We assessed the patient's improvement at each timepoint, determining if there was an increase of at least 25%, 50%, and 75% in 3 or more of the 5 core set measures.
2) Skin sclerosis assessment
   A The mRSS is a widely used clinical tool for assessing skin fibrosis in systemic sclerosis (SSc). It involves palpating and scoring the skin thickness on a scale of 0 to 3 at 17 body areas, with the total score ranging from 0 (normal skin) to 51 (severe thickening in all areas). Skin sclerosis was assessed by mRSS by two separate physicians at each observation points.
   B Ultrasound (US) and shear wave elastography (SWE) examinations conducted. These examinations were performed by one musculoskeletal sonographer (G.L.H) using the Aixplorer US system (SuperSonic Imagine, Aix en Provence, France). The same linear-array transducer (frequency, 4-15 MHz) with preset musculoskeletal (MSK) parameters was used to obtain B-mode US, color Doppler US (CDUS), and SWE images. The arm, thigh, and leg of patients were examined in longitudinal planes, and SWE images of the target were obtained without changing the patient's position. The elasticity range used was 0 (blue, soft) - 600 (red, hard) kPa. A square region of interest (ROI) was set in the dermis to obtain the SWE images. The maximum (Emax), mean (Emean), minimum (Emin), and standard deviation (ESD) elasticity values were automatically presented in kPa. Triplicate measurements were performed on the target, and the mean (Emean) elasticity values were calculated for statistical analysis.
3) Interstitial lung disease assessment
   A Interstitial lung disease was assessed through a comprehensive evaluation that included chest computed tomography (CT) scans and pulmonary function tests.
   B Serum levels of Krebs von den Lungen-6 (KL-6; normal range: 0-460 U/mL) were also measured as using the chemiluminescence method.
4) Evaluation of cardiac involvement
   A Besides patient's electrocardiogram (ECG/EKG) to identify irregular heart rhythms, ischemic changes, and other abnormalities, a comprehensive evaluation of cardiac fibrosis was taken.
   B Echocardiogram was used to assess heart function, measure ejection fraction, and detect any structural abnormalities.
   C Cardiac magnetic resonance (CMR) is used to detect cardiac tissue changes and especially to quantify myocardial fibrosis. Late gadolinium enhancement (LGE) LGE imaging method was employed to detect of fibrous lesion. CMR parametric T1 mapping, are quantitative magnetic resonance imaging techniques that provide a pixel-by-pixel map of precisely numerical T1 values, act as surrogates for diffuse fibrosis on the premise of detecting myocardial water in the expanded interstitial space. This measurement was performed by sophisticated radiologists.
5) Skin biopsy histopathology
   A Skin biopsies were performed at baseline and the third month from the lateral side of the right forearm of the patients.
   B The skin tissue was fixed in 4% paraformaldehyde and then processed for paraffin embedding. The tissue sections were stained with hematoxylin and eosin for histopathological examination. Nuclei are stained a distinct blue with Hematoxylin, while the cytoplasm is stained varying shades of pink to peach with Eosin. Collagen deposition in the dermis was observed using Masson staining. Collagen fibers appear blue, cytoplasm appear red, and nuclei are stained blue-black.
   C Multicolor immunofluorescence histochemistry (mIHC) was employed both before and after therapy to detect the deposition of TGF-beta. This was achieved using a TGF beta 1 antibody (Abclone, A2124) at a dilution of 1:1000.

Additionally, CK5/6 was utilized as a marker for identifying basal and squamous cells in the skin, employing the CK5/6 antibody (ZSGB-BIO, ZM-0313).

D The CD19 positive cell infiltration was tested by immunohistochemistry using CD19 antibody (ZSGB-BIO, TA-506236) to indicate B cell in skin tissue.

E The PANNORAMIC MIDI II (3DHISTECH Ltd.) is utilized for the automated scanning of slides and acquisition of images.

Safety monitoring

1 The patient's temperature and vital signs were recorded at each time point under the same circumstances.

2 Routine examinations of blood cell count, lymphocyte subsets; and biochemical indices of liver, kidney, and heart function were conducted during regular follow-ups. These tests were conducted by the professional technical staff at the Medical Laboratory Center of Shanghai Changzheng Hospital, following the instructions provided in the test kit manuals.

3 C-reactive protein (CRP) was quantified by immunoturbidimetry. The test was conducted by the professional technical staff at the Medical Laboratory Center of Shanghai Changzheng Hospital, following the instructions provided in the test kit manuals.

4 The concentrations of various cytokines in the supernatants of peripheral blood mononuclear cells were precisely quantified. This measurement was performed using immunofluorescence analysis on a BD FACSCalibur system. The analysis was conducted at Hangzhou Dian Medical Laboratory Center, and the reagent kits were supplied by CELLGENE BIO.

5 The patient was closely monitored throughout the entire process for potential adverse events previously reported in other UCART studies, including CRS, ICANS, and GVHD.

1) The safety evaluation was conducted using the NCI-CTCAE 5.0 standards.
2) For CRS, the ASTCT Consensus Grading Standards were employed.
3) The assessment of ICANS was based on the Adult ASTCT ICANS Consensus Grading Standards.
4) Acute GVHD was graded according to the 2016 Mount Sinai Acute GVHD International Consortium criteria, while chronic GVHD was evaluated using the standards set forth in the 2020 NCCN Guidelines for Hematopoietic Stem Cell Transplantation, 1st Edition.
5) The skin pathological manifestations of GVHD, including epidermal degeneration, interface dermatitis, dermal inflammation, hair follicle damage, dermal sclerosis, and adnexal atrophy, were further evaluated using the aforementioned hematoxylin-eosin staining and multiplex immunohistochemistry (mIHC).

QUANTIFICATION AND STATISTICAL ANALYSIS

Flow cytometry data analysis

Population frequencies were analyzed and exported by CytExpert 2.4. Summary plots were prepared using OriginPro 2022 (SR1).

Processing of whole-genome-sequencing data

For WGS bioinformatics, raw reads were filtered using fastp (Version 0.19.5). Clean reads were aligned to the reference human genome (GRCh37) using BWA (version 0.7.12), then the mapped reads were sorted and indexed with SAMtools (Version 1.4). To generate analysis-ready BAM files, recalibration of base quality scores, single nucleotide polymorphism (SNP) and insertion/deletion (INDEL) realignment were performed using GATK (Version 4.1.0.0), while duplicate reads were marked using Picard (Version 4.1.0.0). Variant calling was conducted using these final BAM files, with reference to several annotation databases such as Refseq, 1000 Genomes, the Catalogue of Somatic Mutations in Cancer (COSMIC), OMIM, etc. ANNOVAR was used for annotation. Copy number variation (CNV) was inferred from sequencing data using CNVkit (Version 0.9.5), while structural variation (SV) was called using Lumpy software (Version 0.2.13). The resulting genomic variation information was visualized using a Circos diagram.

Bioinformatics analysis of GUIDE-seq and SITE-seq data

Data was analysed using open-source GUIDE-Seq software and followed the suggested analysis pipeline (v1.0.2; GitHub-aryeelab/guideseq: Analysis pipeline for the GUIDE-seq assay.) and protocol for analysing data from SITE-Seq (version 1 posted 01 May, 2017; https://protocolexchange.researchsquare.com/article/nprot-5889/v1).

Bioinformatics analysis of PEM-seq data

Fastp software (Version 0.23.2) was performed to remove low-quality reads from the raw sequencing data. This included removing reads with adapters, reads with unqualified bases (mass less than 20) accounting for more than 10%, and reads with a length less than 50 bp. The output of this process was high-quality clean reads, which were then used for downstream bioinformatics analysis.

The PEM-Q pipeline (2021.1.12), designed for analysis of PEM-seq (https://www.nature.com/articles/s41421-019-0088-8/), was utilized to identify various genome editing products, such as perfect rejoinings, indels, translocations, and other chromosomal abnormalities. PEM-Q required 8 parameters: reference genome, Sample Name, sgRNA cut site position, sgRNA target chromosome, primer start position, primer end position, primer_strand, and primer_sequence. Break-site and neighbor ±10 bp region was analyzed for indels; reads containing large deletions resulting from resection and rejoining in the break-site ±500 kb region were also

categorized as indels (I). Reads without any detected mutations around break point were identified as germline (G). Reads containing sequences which can be aligned to different positions was analyzed for Genome-wide translocation (T). The junctions can be on the break-site chromosome, but out of the +/-500 kb around the break-site or junctions on other chromosomes. The editing efficiency was calculated as bellow:

$$\text{Editing efficiency} = \frac{I+T}{I+T+G}$$

For off-target analysis, translocation hotspots with sequences very similar to that of the target site ($\leq$7 nt mismatches, including both the spacer and PAM sequences) and with more than 3 junctions at the presumed cut-site were considered off-target sites. Additionally, translocation junctions within 100 bp of the detected off-target site were regarded as off-target translocations.

T1 mapping analysis of CMR imaging

T1 mapping was performed using the modified Look-Locker inversion recovery (MOLLI) sequence. The MOLLI sequence was acquired in three short-axis views of the left ventricle (basal, mid, and apical short-axis planes). The imaging parameters for the T1 mapping were as follows: matrix = 192×192, slice thickness = 8 mm, TR/TE = 2.9/1.5 ms.

All CMR images were analyzed by independently 2 radiologists independently using the professional commercial post-processing software AW4.7 (GE Healthineers, USA). The mean T1 values for each segment on the basal, mid, and apical short-axis slices of the left ventricle were then calculated and used for visualization.[59] The data were visualized using a polar coordinate system in ggplot2 in R, generating a bull's-eye plot. In this plot, the inner ring represents the apex, the middle ring represents the mid segments, and the outer ring represents the basal segments.

Statistical analyses

This clinical trial, involving 3 patients, utilized descriptive statistics to report specific parameters at baseline and at each follow-up timepoint.

ADDITIONAL RESOURCES

All data presented in this manuscript are from the clinical trial NCT05859997. https://clinicaltrials.gov/.

CellPress

Supplemental figures

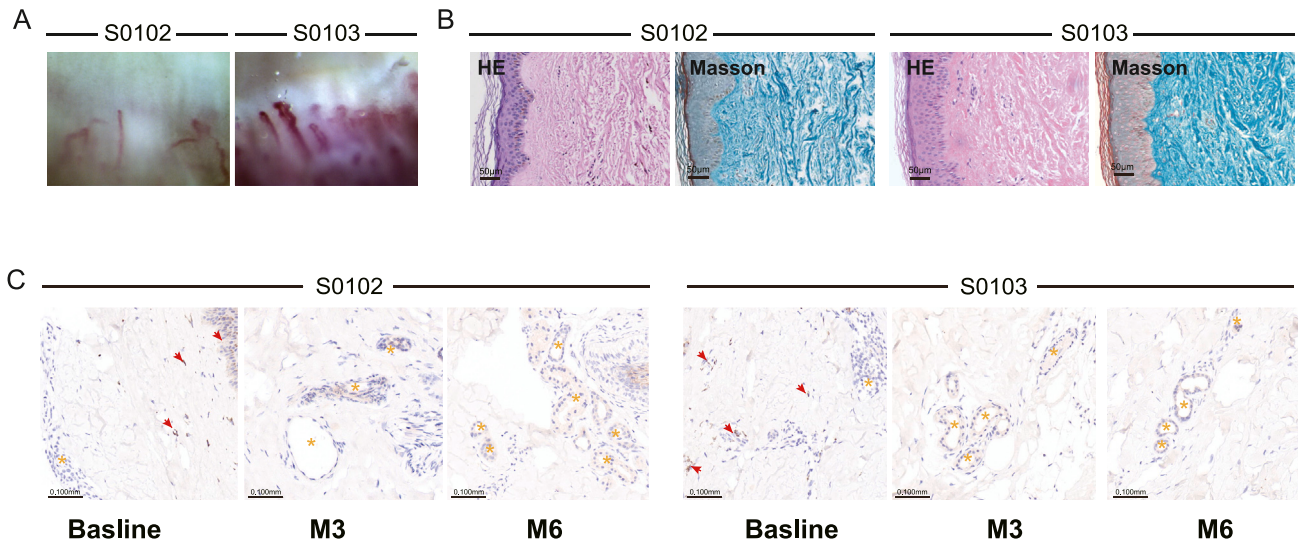

Figure S1. Nailfold capillaroscopy evaluation, skin pathology, and CD19 immunohistochemistry in the two dcSSc patients, related to Figure 3

(A) Nailfold capillaroscopy evaluation for microvascular abnormalities. Left, patient S0102; right, patient S0103.

(B) Pre-treatment histopathological manifestations of the upper limb skin as revealed by H&E staining (method details). Changes in the arrangement of collagen fibers as revealed by Masson's trichrome staining. Scale bars,100 μm.

(C) Anti-CD19 immunohistochemistry (IHC) (method details) of skin biopsy collected at baseline, 3 months, and 6 months after receiving TyU19 CAR-T treatment. B cell infiltration (marked by red arrows); normal and regenerated cutaneous appendages (marked by yellow stars).